Faculté des Bioingénieurs

Dehydration of ethanol over hydrophobic hybrids of niobium-silica mixed-oxides prepared by non-hydrolytic sol-gel process

Présenté par Gautier Boogaerts

Promoteurs : Prof. Damien Debecker (UCL/MOST)
Dr. Ales Styskalik (UCL/MOST)

Lecteurs : Prof. Michel Devillers (UCL/MOST)
Prof. Carmela Aprile (UNamur/NISM)

Mémoire de fin d'études présenté en vue de l'obtention du diplôme de **Bioingénieur : chimie et bioindustries**

Année académique 2017-2018

Acknowledgements

This master's thesis could not have been completed without the help of several people who knew how to transmit their knowledge and experience. Their constructive comments and their wise advices allowed me to elaborate this work.

First, I would like to express my sincere gratitude to my advisor Prof. Damien Debecker for the continuous support of my master's thesis, for his patience, motivation, and immense knowledge. His guidance helped me in all the time of research and writing of this work.

I would also like to thank my co-advisor Dr. Ales Styskalik. The door of his office was always open whenever I ran into a trouble spot or had a question about my research or writing. He consistently followed my work and steered me in the right direction when I needed it the most.

I thank my fellow 3C mates for the daily laughs, for the sleepless nights we were working together before the final deadline, and for all the fun we had in the last five years. Merci à vous les potes. Merci à mes parents et à ma petite soeur d'avoir été là pour moi pendant la réalisation de ce mémoire. Merci aussi à Maud de m'avoir supporté malgré mon manque de sommeil durant les dernières semaines. Enfin, je remercie sincèrement Martin, Tanguy et mes compagnons de l'Antre, vous êtes une inspiration quotidienne pour moi.

Finally, I must express my very deep gratitude to everyone who was involved in the writing of this master's thesis, and to the daily good mood of everyone in the lab.

Abstract

The production of bio-sourced compounds has been deeply investigated during the past few decades as an alternative to the petrochemical industry. Currently, the main pathway to produce ethylene, one of the most produced chemical compounds in the world, is through hydrocarbon cracking process. Because of the depletion of fossil fuel reserves and their harmful impact on the global warming, the use of biomass **ethanol catalytic dehydration** has been developed. Various heterogeneous catalysts for this dehydration reaction have been explored, but poor resistance in high water concentration was reported. However, new **niobium-silica mixed-oxides** (**Nb_2O_5-SiO_2**) materials in recent research have displayed high hydrothermal stability while showing good catalytic performance. In line with it, hybridization (*i.e.: incorporation of organic moieties*) of this promising catalyst has been investigated in this work to make it even more resistant against hydrolysis. Another suggested feature of hydrophobic hybrids is that water, created during dehydration reaction, would desorb easier from the surface of the solid and thus impact the catalytic activity.

In this study, novel preparation method, the **non-hydrolytic sol-gel** (**NHSG**) process has been applied as it largely improves the homogeneity of the synthesized solids, which is an important property of hybrid mixed-oxides. Furthermore, this particular technique usually produces mesoporous materials with high specific surface areas. Two synthetic NHSG pathways have been studied in this work: (i) the alkyl halide elimination and (ii) the acetate route. Hybridization was carried out during the NHSG process by adding different types of organosilane precursors directly into the reaction mixture. Tested organosilanes include aromatic and aliphatic moieties both terminal ($C_6H_5SiR_3$, $(C_6H_5)_2SiR_2$, CH_3SiR_3) and bridging ($R_3SiC_6H_4SiR_3$) (R=Cl (i),OAc (ii)). Different molar ratios of organic groups were used in order to see the influence of their amount on the properties of the material.

In order to understand the stability and the catalytic performances of the hybrids, their physico-chemical characterization has been performed. Surface analyses reported that all synthesized materials were mesoporous with high surface areas. Niobium was successfully incorporated in all cases, however samples from the acetate route have shown a slightly better

homogeneity of niobium dispersion in silica. The overall homogeneity of Nb-Si mixing in hybrids samples decreased with higher loadings of organic groups.

A big part of this master's thesis has been devoted to the evaluation of the catalytic activities in the ethanol dehydration reaction. Samples produced through the acetate pathway display higher conversions than samples from the alkyl halide elimination route. It was found out that high organic content in hybrid catalysts decrease the conversion of ethanol. All types of organic compounds integrated in hybrids behave similarly, except for methylated samples which have a relatively good conversion but show lower ethylene production.

Another objective was to enhance the hydrothermal stability of the samples to make them more economically and ecologically interesting. Indeed, pure ethanol production implies several step of distillation to get rid of the water. If the catalyst stability was improved in presence of water, then these expensive unit operations would be avoided. Unfortunately, when the hybrid samples were exposed to water at 250 °C for 24 hr, significant losses of surface areas and pore volumes were observed. Further research proved that the hydrolysis of the silicon-carbon bond takes place under these conditions. All types of organic compounds have been shown unstable against water, however methylated samples seem to be slightly more stable than catalysts with incorporated aromatic groups.

Table of contents

1. Introduction

1.1 Context

Since the industrial revolution, scientific efforts on energy and transportation has been governed by basic and applied research in the development of petroleum, coal, and natural gas based refinery to exploit fossil feed stocks. Fossil fuel-based industries were also able to produce different types of cheap and necessary products such as fuel, plastics, fine chemicals, pharmaceuticals, pesticides, solvents, etc [1,2]. Fossil fuels were and still are the dominant energy sources, filling 80% of the world's energy demand [3]. However, they are nonrenewable and their reserves are limited. In addition to that, since the total combustion of fossil fuels produces CO_2, one of the most harmful greenhouse gases, this source of energy is directly associated with the global warming observed during the past few decades. The ecological impact induced by fossil fuel together with the decreasing of available sources has opened new alternative research towards potential solutions. As a way to tackle this issue, many new **bio-sources** have been deeply investigated in the last 15 years. It is in this research perspective that the first generation of biofuel (including bioethanol) was born [4,5].

First generation biofuels produced from biomass such as plants or organic waste seemed indeed an interesting alternative, as it could help to minimize the fossil fuel burning and thus to mitigate the CO_2 production. This solution appeared to be promising as it could help to reduce both the world's dependence on fossil fuels and greenhouse gas production. In fact, the CO_2 released in combustion would equal the CO_2 assimilated by the plant during photosynthesis, thus making biofuel a more environmentally friendly energy source. In addition to the reduction of greenhouse gas emissions and to the energy supply security, biofuels could also help boost rural incomes and employment [6]. However, as appealing as this alternative looks, there are concerns about environmental impacts and carbon balances. Actually, the main drawback is the competition existing between this biofuel and the food that could have been produced instead. One of the most important consequences of this is the rising food prices due to the production of these fuels [7].

Since this first generation of biofuels shows unavoidable drawbacks, a second solution emerged: using cellulosic products such as wood, straw, long grass or wood waste, which would not compete with the food production. The main advantage of second generation biofuels is the use of the whole plant (including stem, leaves and peels) and can be produced from plants with no edible part (*Jatropha curcas*, switchgrass, etc.), waste from wood processing and pulp of the fruit [8]. Nevertheless, as far as this solution goes, the problems in the production of second-generation biofuels are the different processes to be able to break down the lignocellulose from these feedstocks. In addition to that, biofuel production from agricultural by-products cannot satisfy the whole world demand for liquid fuels [9]. This suggests that in the future we would have to dedicate crops to produce biofuels. Even if the production of second-generation biofuels is not already fully implemented on the market, a lot of research is being developed to do so, as these biofuels could help reducing CO_2 production, can offer better engine performance in some cases and do not compete with corps dedicated to food production.

Values of these new biofuels are not limited to the feeding of car engines and transportation, as it can also replace chemical products from petrochemistry. For example, **bioethanol**, which is the most commonly used biofuel in the world, can be used to produce several most important petrochemical products such as ethylene or butadiene. These platform products made from bioethanol can be polymerized to form bioplastics that has the same physical and chemical properties as regular plastics while maintaining full recycling capabilities [10].

In order to replace chemical production from fossil fuels, new adapted technologies have to be developed. Bio-based chemical production reactions need a high amount of energy to be carried out, thus the use of catalysts has been investigated. As a matter of fact, catalysts will enhance these reaction rates as they will decrease their activation energy. Strong acids and bases are known as good catalysts for this type of reactions but unfortunately they also have many drawbacks such as toxicity and corrosion, difficulties in the separation between the products and the catalyst and they are very polluting. Solid catalysts are able to tackle these problems by avoiding separation steps, reducing energy consumption and waste generation as well. When solid catalysts are working in gas phase or in liquid phase and are not soluble, they are called **heterogeneous catalysts**. Heterogeneous catalysis is already widely used in petrochemical and

refinery industries, however the differences in composition between fossil resources and biomass requires the development of specific catalysts with ad hoc properties [11]. In this context, the quest for innovative catalyst formulations is still vivid, fostered by original synthetic methods.

1.2 Production of bio-sourced compounds

The conventional approach to convert fossil resources into liquid fuels and chemicals is radically opposed to the one that aims to convert biomass. Hydrocarbons from oil are indeed usually more hydrophobic, rarely contain oxygen, nitrogen or sulfur and are monomeric whereas biomass is based on polymeric compounds that are more hydrophilic and which contain a lot of oxygen species [12]. Thus, the transformation of biomass in liquid fuels requires to reduce the amount of oxygen moieties. Nevertheless, biomass provides an abundant variety of chemical functions, which is interesting in the production of innovative chemical compounds or in the improvement of the already existing compounds on the market (*Figure 1*). This biomass transformation therefore requires catalysts with special properties. The elimination of excess oxygen can be carried out by several reactions such as dehydration, decarboxylation, esterification, condensation reactions, etc [13].

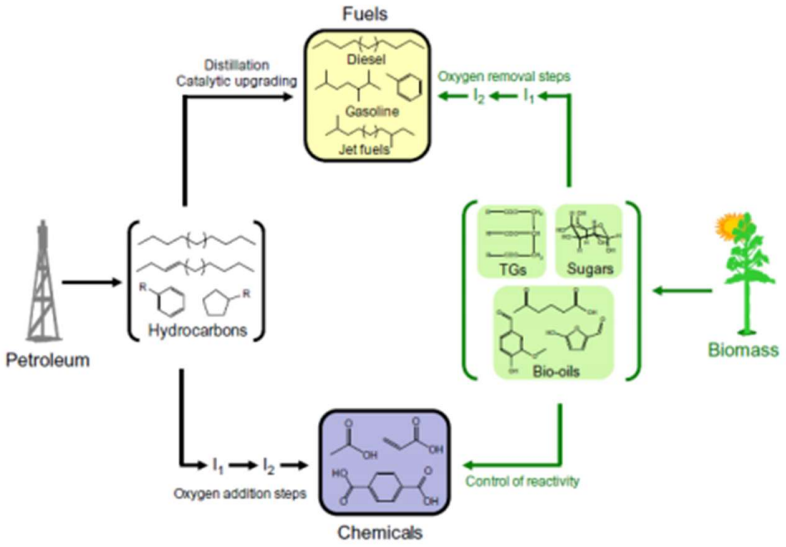

Figure 1 Comparison between different approaches for the conversion of petroleum and biomass into liquid fuels or chemicals [11]

The transformation of biomass into valuable products requires the use of heterogeneous catalysts at different stages. First, heterogeneous catalysts have been investigated for the transformation of raw biomass into intermediate products like bio-ethanol for instance. During the step of transformation of these intermediates, such catalysts are used to produce platform molecules (olefins, acrolein, etc.) which are widely used in the petrochemistry field. However, for this second step, these catalysts must be able to convert highly oxygenated molecules. In order to do so, basic or/and acidic properties of the catalysts can be exploited. With that in mind, one of the key steps during the synthesis of these catalysts will be to control the number and strength of the active sites. The **dehydration of ethanol** illustrates well this case because the catalyst requires a desired balance of density, nature and strength of acidic sites.

1.3 Dehydration of ethanol

Ethylene is one of the most produced chemical compounds in the world and also one of the most important raw materials in the petrochemical industry. As a matter of fact, about 75% of petrochemical products are produced from ethylene, including acetaldehyde, acetic acid, ethylene glycol, etc.; but it can also be used as a platform molecule for the production of polymers such as polyethylene, polyvinyl chloride, etc [14]. The main pathway to produce ethylene now is through hydrocarbon cracking processes, as 99% of the global ethylene is synthesized by this method. Because of the depletion of fossil fuel reserves during the past few decades, new renewable ways to synthesize ethylene have been investigated. To tackle this problem, the use of biomass ethanol catalytic dehydration has been developed [15].

The catalytic dehydration of ethanol produces ethylene, together with diethylether as a main byproduct, but can yield also small amount of other byproducts, such as acetaldehyde [16], hydrocarbons (methane, ethane, propylene, butylene, etc.) [17], and light gases (CO_2, CO, H_2, etc.) [18]. Usually, the amount of these other byproducts is small, and thus the main mechanisms of ethanol dehydration reaction consider only the generation of ethylene + water (*Eq.1*) and diethylether + water (*Eq.2*).

$$C_2H_5OH \rightleftharpoons C_2H_4 + H_2O \qquad (Eq.1)$$

$$2\,C_2H_5OH \rightleftharpoons C_2H_5OC_2H_5 + H_2O \qquad (Eq.2)$$

Nonetheless, the mechanism of ethylene production from ethanol is still controversial. Either the production of ethylene is directly generated from ethanol or generated from diethylether, or both routes just coexist (*Figure 2*).

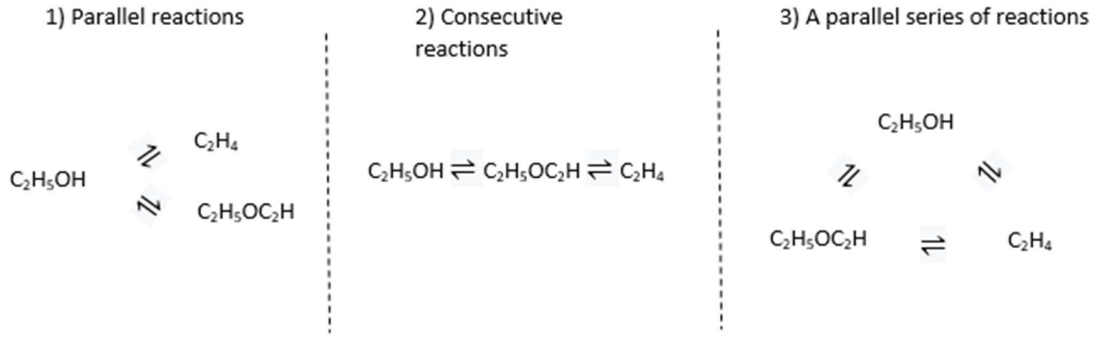

Figure 2 Different reaction pathways possible for the production of ethylene

The mechanism depends mostly on the catalytic conditions and on the nature and density of the acid sites of the catalyst. The selectivity to ethylene and diethylether is indeed strongly affected by the reaction temperature. In many different dehydration reactions (ethanol, 1-propanol, 1-butanol), literature shows that low temperatures favor ether formation, whereas at higher temperatures (250-300 °C) alkene are produced with 100 % selectivity [19]. This could be a clue to the existence of different energy barrier corresponding to different acid sites that could be activated at different temperatures regarding the strength of these sites.

Since the ethanol dehydration to ethylene is an acid catalyzed reaction, several catalysts displaying such acidic properties have been developed like clays, activated alumina, silicon oxides, magnesium oxides, molecular sieves, heteropolyacids, etc. [14]. Recently, **niobium-silicon mixed-oxide (Nb_2O_5-SiO_2)** has attracted great interest for its potential application as heterogeneous catalyst in the dehydration of ethanol [20].

1.4 Nb_2O_5-SiO_2 mixed-oxide catalyst

Materials containing niobium seem to be promising for the conversion of bio-based compounds, as their stability in hydrothermal conditions and their reactivity are particularly interesting [20]. The particularity of Nb oxides and their derivatives is that their acido-basic properties can be modified by their hydration rate, thus hydrothermal treatments and the atmosphere surrounding the catalyst can modify the activity of the sample. Among all the niobium based materials, Nb_2O_5-SiO_2 is reported in the literature as a good catalyst for dehydrations reactions but also hydration, condensation and epoxidations reactions [21]. As opposed to the pure oxide catalyst Nb_2O_5, the homogeneous mixed-oxides can generate new active sites of different nature and strength. The niobium silicate mixed-oxide has shown both Lewis and Brønsted acidity [20]. Furthermore, in the case of this mixed-oxide, Nb seems to improve the hydrothermal stability [22].

In anhydrous conditions, Nb_2O_5-SiO_2 with a low niobium loading (below 10%) mainly possesses isolated NbO_4 species, which are displaying weak Lewis acidity (*Figure 3*) [23]. However, with higher Nb loadings, more Brønsted acid sites appear on the surface. These can be associated with the production of bulk niobium oxide, and literature shows that these Brønsted acid sites from bulk niobia are much less active than the isolated NbO_4 species [24]. In hydrated conditions, *Frederik and al.* [25] observed that for Nb isolated in silica in substituted zeolites, there is a competition between Nb-OH (*Figure 4)* (Brønsted acid sites) and Nb=O (Lewis acid sites). Metastable sites such as Nb=O...H_2O and Nb-OH…H_2O are also likely to appear in aqueous media. The coordination of a water molecules on these sites can modify the nature and the strength of the acid site, thus modifying the overall acidity of the catalyst. Therefore, these sites can be altered when exposed to water [26].

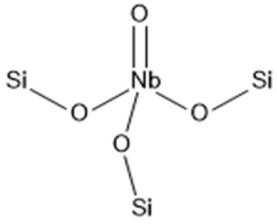

Figure 3 Lewis acid sites in Nb_2O_5-SiO_2 mixed-oxide

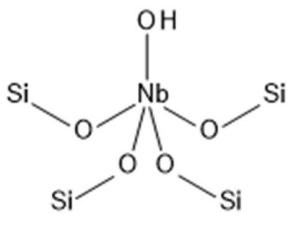

Figure 4 Brønsted acid sites in Nb_2O_5-SiO_2 mixed-oxide

Yet, to obtain a catalyst with these desired acid sites, it is necessary to have a homogeneous mixed-oxide, and therefore requires new particular synthesis methods. During the last 25 years, **the non-hydrolytic sol-gel (NHSG)** synthesis processes were found to be attractive and versatile method for the preparation of homogeneous mixed-oxides with good textural properties (mesoporous materials with high surface areas) [27]. This synthesis method is an extension of the classical well-known sol-gel method.

1.5 "Classical" sol-gel approach

The term "sol-gel" was first used to describe hydrolysis and condensation processes, but with the progress in this field during these last few years, the initial use of the term is now valid for a broad range of different reactions. Nowadays, the sol-gel process can be defined as the preparation of inorganic polymers or ceramics from a solution through a transformation from precursors to a "sol"[1] which then converts into an integrated network called a "gel". Sol-gel chemistry is now an important toolbox for the preparation of heterogeneous catalysts [28].

Most of the sol-gel chemistry is based on metal (M) alkoxides, but it can also occur between hydrated metal species. The early p-block elements (e.g.: Al, Si) and some transition metals of d-block (e.g.: Ti, Zr, Nb) are examples of alkoxide-based sol-gel chemistry. These metal-alkoxides will have to go through several steps to yield a porous solid material (*Figure 5*). First, molecular precursors reacts to form a colloidal suspension and then a gel (sol → gel). The gel is constituted of a 3D-reticulated solid network within the solvent, condensation residues (HOR and H_2O) and precursors that have not reacted yet. The condensation reactions can proceed and thus increase the degree of crosslinking of the oxide, resulting in syneresis phenomena and in the partial shrinking of the gel. The gel is then dried to evaporate the liquid phase containing organic residues. If the drying of the gel corresponds to an evaporation of solvent, a loss of porosity caused by the collapsing of the walls can occur. In some cases, this loss may not be significant, and a xerogel[2] is formed. It is possible to preserve the porosity by drying under supercritical CO_2, yielding an aerogel. However, this method is complex and expensive. Alternatively, sacrificial

[1] The "sol" is a colloidal suspension of very small solid particles in a continuous liquid medium.
[2] "Open network formed by the removal of all swelling agents from a gel." – IUPAC definition

templating agents can be used to generate porosity [28,29]. Finally, a calcination step is required to get rid of all the remaining unreacted residues.

Figure 5 Overview of the sol-gel process

The synthesis of the colloidal suspension is an important step that goes through several different reactions. These reactions have to be well understood in order to control the process of sol-gel chemistry. In classical hydrolytic sol-gel processes, metal alkoxides such as tetraethyl orthosilicate (TEOS) yield a sol by going through hydrolysis (*Eq.3*) and condensation (*Eq.4*, *Eq.5*) reactions:

$$-\mathrm{Si}-\mathrm{OR}+\ \mathrm{H_2O}\rightarrow\ -\mathrm{Si}-\mathrm{OH}+\mathrm{HOR} \qquad (Eq.3)$$

$$-\mathrm{Si}-\mathrm{OH}+\mathrm{HO}-\mathrm{Si}-\ \rightarrow -\mathrm{Si}-\mathrm{O}-\mathrm{Si}-\ +\mathrm{H_2O} \qquad (Eq.4)$$

$$-\mathrm{Si}-\mathrm{OH}+\mathrm{RO}-\mathrm{Si}-\ \rightarrow -\mathrm{Si}-\mathrm{O}-\mathrm{Si}-\ +\mathrm{ROH} \qquad (Eq.5)$$

The possibility and the ease with which the sol-gel chemistry is possible depends on several factors. The first parameter to take into account is how the electronegativity differences between the oxygen and the metal affects the nature of the M−O bond. Aside from the electronegativity factor, the effect of electron donating/withdrawing ability of the alkyl chain (R) can influence the stability of the alkoxy- groups. Both of these factors have an important effect on the final gel structure by changing the relative rates of hydrolysis and condensation and thus the degree of polymerization as well. Mixed-oxides can be synthetized by a similar process, involving different molecular precursors. As an example, for the incorporation of niobium through sol-gel synthesis, TEOS and $Nb(OEt)_5$ can be used as precursors [30]. Niobium precursors can either condense with silicon precursors (*Eq.6*) yielding a mixed oxo-bridge, or react with themselves (*Eq.7*). The homogeneity of the materials – in terms of Nb dispersion into the silica matrix – will depend on the relative proportions of each bonding types.

$$-\mathrm{Nb}-\mathrm{OH}+\ \mathrm{HO}-\mathrm{Si}-\ \rightarrow\ -\mathrm{Si}-\mathrm{O}-\mathrm{Nb}-+\mathrm{H_2O} \qquad (Eq.6)$$

$$-\mathrm{Nb}-\mathrm{OH}+\ \mathrm{HO}-\mathrm{Nb}-\ \rightarrow\ -\mathrm{Nb}-\mathrm{O}-\mathrm{Nb}-+\mathrm{H_2O} \qquad (Eq.7)$$

Therefore, in order to obtain a homogeneous mixed-oxide, metal precursors has to react preferably with silicon precursors. However, the majority of metal precursors are very reactive while silicon precursors are more stable. Nb species will be more likely to hydrolyze and react more quickly than the silicon precursors, producing a heterogeneous oxide. Differences between reaction rates is a barrier against the preparation of homogeneous mixed-metal-oxides. Moreover, water can be a problem during the drying of the gels as capillary forces can lead to pore collapse. Materials resulting from hydrolytic sol-gel process are usually microporous.

1.6 Non-hydrolytic sol-gel (NHSG) process

Many alternatives have been developed to overcome issues related to the sol-gel method [31]. Among them, one improvement was to use an oxygen donor other than water (e.g.: alkoxides, ether, alcohol, etc.) by switching to a non-aqueous media. This method was given the name of non-hydrolytic sol-gel process and was shown to be advantageous in many applications, such as in the preparation of organic-inorganic hybrid mixed-oxides [32]. Moreover, reactions rates in NHSG are generally lower in comparison to hydrolytic sol-gel. Since the reactions are slower, they are easier to control and organic compounds are more dispersed into the hybrid. Last but not least, non-hydrolytic (NH) gels are usually able to withstand capillary stresses generated by the solvent evaporation and to retain a high pore volume during drying, even without using supercritical conditions. This capacity has been attributed to the high degree of condensation, conferring a high mechanical strength to NH gels with respects to hydrolytic ones. Furthermore, the capillary forces are likely reduced due to the low surface tension of the liquid phase compared to water, leading to mesoporous materials with surface area as high as 1000 m^2 g^{-1} [31]. Several non-hydrolytic synthetic routes involving reactions of precursors (chlorides, alkoxides, etc.) with oxygen-donors (alkoxides, ethers, alcohols, etc.) have been described in the literature. This study is limited to two different routes of synthesis: The alkyl halide elimination and the acetate route.

1.6.1 "Alkyl halide elimination" route

The "alkyl halide elimination" route is one of the most used methods to prepare catalytic materials by NHSG process [31]. It is based on the reaction of chloride precursors with alkoxides, ethers or alcohol oxygen donors, resulting in an elimination of alkyl chloride. Diisopropylether is usually used as the oxygen donor as it forms a relatively stable carbocation and this feature facilitates condensation reactions. Therefore, the use of diisopropylether leads to short gelation times and high degrees of condensation [33].

Niobium pentachloride ($NbCl_5$), as the niobium precursors, first react with diisopropylether, producing niobium alkoxide chloride and isopropyl chloride (*Eq.8*). Then, two possible reactions can happen simultaneously. Either the chloro-alkoxy-niobium species react with silicon tetrachloride ($SiCl_4$) (*Eq.9*) or with the remaining niobium pentachloride (*Eq.10*). In both cases, there is again an elimination of isopropyl chloride.

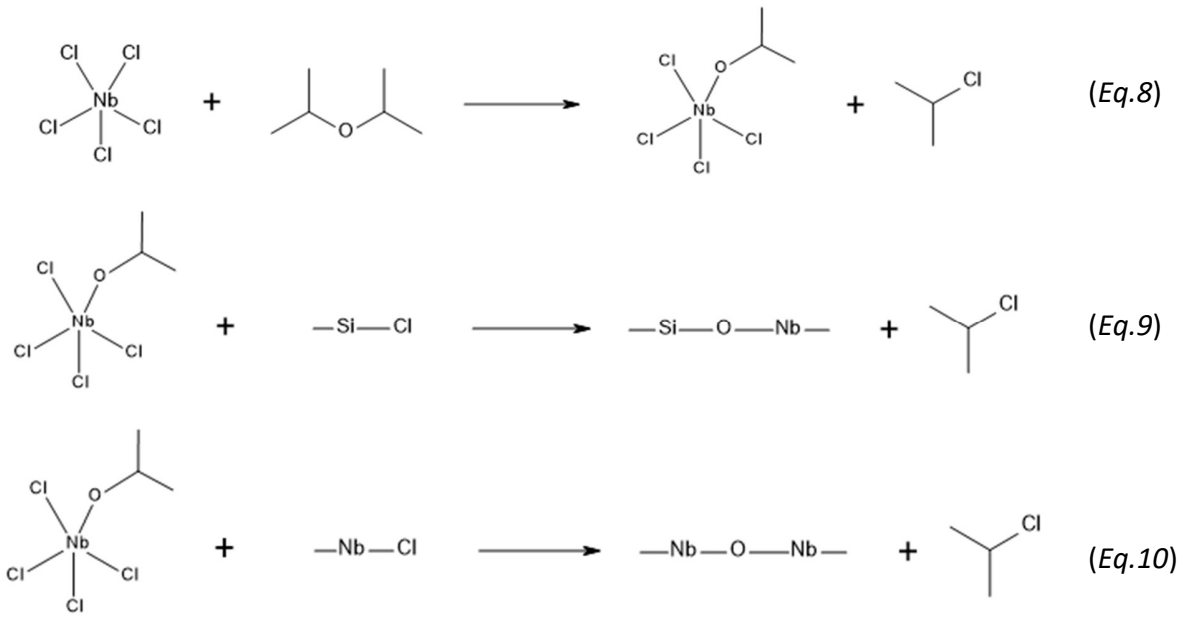

The alkyl halide elimination route has been used for the preparation of a wide variety of metal oxides and has proven useful for the synthesis of binary mixed-oxides as it gives a good control over the homogeneity and the texture of the samples [34]. Moreover, the synthetic

pathway is simple, as it only requires metal chlorides and ether (no alkoxides) and yields high surface area materials.

1.6.2 Acetate route

The acetate route is related to the acetamide elimination route, a well-known reaction in non-hydrolytic sol-gel process [35]. The acetamide elimination route produces highly porous and homogeneous metallosilicates and is based on the reactions of acetoxysilanes with metal amides. This process usually yields a high number of M−O−Si bonds as well as dialkylacetamide as a volatile organic product (*Eq.11*).

$$-\mathrm{M}-\mathrm{NR}_2+\ -\mathrm{Si}-\mathrm{OC(O)R'}\rightarrow\ -\mathrm{M}-\mathrm{O}-\mathrm{Si}-\ +\mathrm{R'C(O)NR}_2 \qquad (Eq.11)$$

However, the acetamide route requires the use of a metal amide. Metal amides are usually difficult to operate with because they are highly reactive and their low melting point makes the manipulation of the crystal laborious, as they melt at room temperature (or below). Moreover, only high contents of metals in silica were possible to prepare because of the lack of homocondensation between silicon species (formation of Si−O−Si bridges) (*Eq.13*), resulting in less homogeneous samples. Therefore, slight changes to the acetamide elimination route were suggested in order to increase its applicability: (i) The use of metal chlorides, which are readily available and do not require any preparation of precursors, and (ii) the application of higher temperatures and pressures in an autoclave, which allows for homocondensation of acetoxysilanes and thus the formation of Si−O−Si bonds.

Niobium pentachloride, for instance (same precursor as for the alkyl halide elimination route), reacts with silicon tetraacetate producing Si−O−Nb bonds along with acetyl chloride as a volatile organic byproduct (*Eq.12*). Moreover, if the ratio of Si/Nb is high enough, a high amount of Si−O−Si bonds (*Eq.13*) can be achieved at temperatures ≥ 130 °C, thus yielding siliceous materials with homogeneously dispersed NbO_4 species (*Figure 3)*. A high degree of Si−O−Si bonds also makes xerogels more stable against shrinkage and therefore more porous. This type of bond is produced by the homocondensation of silicon tetraacetate, yielding also acetic anhydride (*Eq.13*).

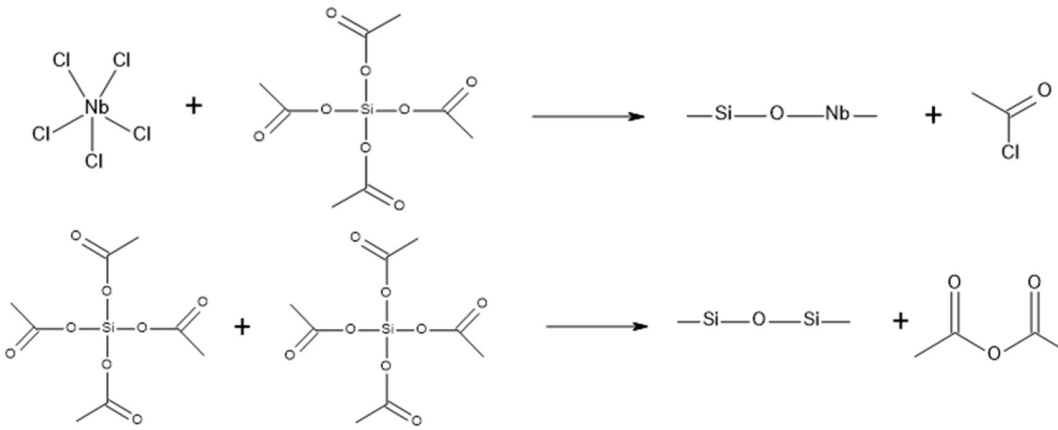

(*Eq.12*)

(*Eq.13*)

1.7 Enhancing of the hydrothermal stability

Since the targeted reaction in this study is a dehydration, the catalyst must show a good performance and stability in the presence of water. Water is a by-product of the dehydration reaction and can have harmful effects on material depending on the temperature and pressure. Moreover, water could come from the (bio)ethanol feed itself. Indeed, to produce ethanol absolute, the removal of water through distillation steps is required. To stay in an eco-friendly perspective, the improvement of the hydrothermal stability of the catalysts could help reduce costs associated to the production of cheaper ethanol by avoiding these distillation steps.

In the case of a mixed-oxide (e.g.: Nb_2O_5-SiO_2), water coupled with a high temperature can cause different effects such as:

- The hydrolysis of the Si−O−Si and Si−O−Nb bridges or Nb−O−Nb which can transform acidic Lewis sites into Brønsted ones.
- A high degree of hydrolysis of the oxo-bridges can weaken the network by producing Si-OH (or Nb-OH).
- Modifying the structure and the texture.
- Alter the surface reactivity by causing the migration of active species (especially at high temperatures).

Nevertheless, strategies have been developed to avoid these issues:

- Using doping heteroatoms in the oxide network (Nb, for instance, has itself a known stabilizing effect on silica [20]).
- **Incorporation of organic moieties** in the oxide network to form a hybrid material; C-C bonds are supposed to be much more stable against hydrolysis.
- Surface modification by functionalization of the silanols with $MeSiO_3$ groups (e.g. by methyltrimethyloxysilane (MTES)) which increases the hydrophobicity of the surface and prevent noxious effects caused by the water.

Among all these strategies to enhance the hydrothermal properties of the material, a particular attention has been given to the preparation of hybrid organic-inorganic niobium-silica mixed-oxides, with organic moieties incorporated inside their framework.

1.8 Incorporation of organic moieties inside an inorganic framework.

In the past few decades, the preparation and processing of organic-inorganic hybrid materials has attracted a great deal of interest in both the academic and industrial world [36]. The properties of hybrid materials do not simply result from the addition of the individual contributions of their components, but also from the strong synergy created by a large hybrid interface. This organic-inorganic interface[3] plays a key role in modulating of a wide variety of properties (optical, mechanical, separation, catalysis and stability to chemical and thermal stresses). Literature has already explored the hybridization of amorphous silica in humid environments, where presence of organic groups was found to have a significant effect in terms of increasing the hydrophobicity of the silica [37].

Hybrids materials can be extended to other applications. In this case the incorporation of organic hydrophobic moieties inside an inorganic mixed-oxide has two preponderant roles: (i) enhance the stability against water and temperature (C-C bonds are supposed to be more stable) and (ii) increase desorption of water during the dehydration process, thus intensifying the reaction rate.

[3] "Nature of interactions, energy and linkability" [36]

1.9 Objectives of the study

This master's thesis aims at developing novel types of heterogeneous acid catalysts with good performances in ethanol dehydration, and with improved hydrothermal stability. More precisely, we will focus on mesoporous niobium-silica catalysts and attempt to demonstrate that their properties can be advantageously tuned using NHSG routes.

First of all, we will aim at materials with interesting textural properties: (i) high surface area to optimize the interactions between reagents and active sites on the catalyst surface, and (ii) large mesopores to allow the approach of the ethanol molecule to the active sites.

Secondly, we will target acidic materials (both in strength and amount of acid sites) and to that end, the homogeneity of the Nb-Si mixed-oxide will be an important objective. Niobium has to be thoroughly integrated and well dispersed inside the silica to form the desired active sites.

Furthermore, we aim at incorporating organic groups inside the inorganic framework of the catalysts and we hope to demonstrate a potentially beneficial effect of such hydrophobization on the catalytic performance and/or on the stability of the catalysts.

Finally, it will be interesting to identify and optimize the type and the quantity of organic moieties to improve the catalysts behavior.

1.10 Strategies

An experimental strategy has been adopted to accomplish these different objectives (*Figure 6*).

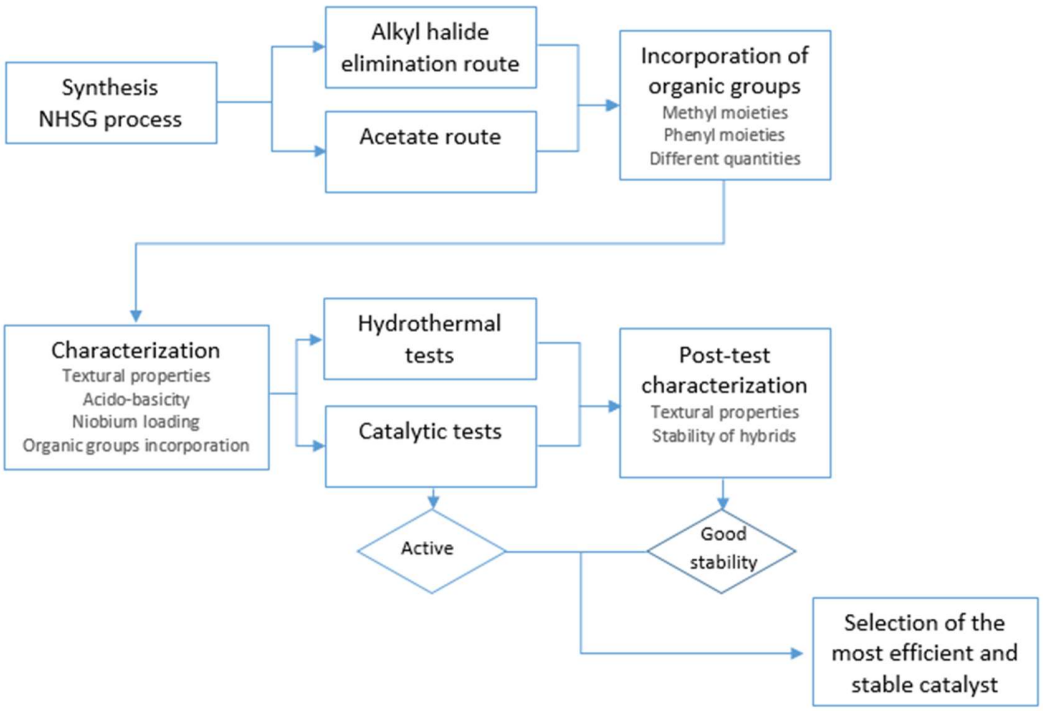

Figure 6 Experimental strategy

First of all, the strategy adopted is to synthesize materials *via* non-hydrolytic sol-gel process. This method was chosen because it produces mesoporous samples with a high degree of homogeneity (important in the study of mixed-oxides), and easily allows for the incorporation of organic groups inside the mixed-oxide [61]. Two different synthetic pathways are investigated: (i) alkyl halide elimination and (ii) acetate routes. Different organosilanes precursors are tried: (i) phenyl groups (pending-diphenyl, pending-phenyl, and bridging-phenylene) and (ii) methyl groups (pending-methyl). Several molecular ratios of these organosilanes precursors are tested in order to see the influence of both the nature and the content of organic groups on the materials.

Once the catalysts are prepared, different characterization techniques make it possible to obtain a physico-chemical description of their properties and to measure several parameters that could play a preponderant role in the catalytic process. The smooth progress of the synthesis can then be verified and the catalysts can be compared in order to relate their properties and behavior in the different tests performed afterwards.

Synthesized catalysts will be indeed submitted first to reaction tests in order to identify their performances. In a second time they will be exposed to hydrothermal tests to determine the stability of the hybrid samples compared to pristine samples. The hydrothermal tests will be performed by exposing the samples to a high water content atmosphere at 250 °C for 24 h, followed analyses verifying the effects of both tests on prepared materials. The stability of each sample will be deduced based on these data.

Finally, materials which possess both good performances and improved stability in hydrothermal condition will be highlighted as potential candidates for further research.

2. Material and methods

2.1 Material

Niobium (V) chloride ($NbCl_5$; ≥99.5 %), Methyltrichlorosilane (CH_3SiCl_3; 99 %) and Molecular sieves (4 Å, beads, 4-8 mesh) come from Sigma-Aldrich. Silicon (IV) chloride ($SiCl_4$; 99.8 %), Dichlorodiphenylsilane ($(C_6H_5)_2SiCl_2$; ≥ 97 %), Acetic anhydride ($C_4H_6O_3$; 99+ %), Sodium (Na; 99.8 %), Phosphorus pentoxide (P_4O_{10}; 98 %) and Pyridine (C_5H_5N; 99 %) come from Acros Organics. Toluene (TOL, ≥99.5 %), Dichloromethane (CH_2Cl_2; ≥99.8 %), Diisopropylether (iPr_2O; ≥98 %), Glass beads (diameter: 0.75-1 mm) and Thionyl chloride ($SOCl_2$; ≥98 %) come from Carl Roth. Benzyl(trichloro)silane ($C_7H_7Cl_3Si$; 97 %) and 1,4-Bis(triethoxysilyl)benzene(BTESB; 95%) come from ABCR. Ethanol (absolute, C_2H_6O, 100 %) come from VWR.

2.2 Methods

2.2.1 Synthesis of precursors

2.2.1.1 Silicon tetraacetate

Silicon tetraacetate was prepared according to *Baltis et al*. work [38]. Silicon tetrachloride (24.28 g, 0.1429 mol) was mixed with acetic acid anhydride (59.51 g, 0.5829 mol, 15 % excess) in inert atmosphere (*Eq.14*). Colorless crystals of $Si(OAc)_4$ grew in the reaction mixture overnight. The liquid phase was removed by a syringe. The product was dried *in vacuo* at room temperature. The reaction produced 28.23 g of silicon tetraacetate (white crystals, yield: 74.88 %).

$$SiCl_4 + 4\ CH_3C(O)OC(O)CH_3 \rightleftharpoons Si(OC(O)CH_3)_4 + 4\ CH_3C(O)Cl \qquad (Eq.14)$$

2.2.1.2 1,4-Bis(trichlorosilyl)benzene

1,4-Bis(triethoxysilyl)benzene (10 g, 0.025 mol) was mixed with thionylchoride (70.9 g, 0.5959 mol, chlorinating agent, 300 % excess) and with pyridine (0.6 g, 7.585×10^{-3} mol) as a catalyst for this reaction (*Eq.15*). The reaction mixture was heated up to 74.6 °C for 48 h under

reflux condenser. The volatiles were removed *in vacuo* and the product was purified by vacuum sublimation at 70 °C (oil bath), producing 5.535 g of 1,4-Bis(trichlorosilyl)benzene (white crystals, yield: 64.20 %). 1,4-Bis(trichlorosilyl)benzene was analyzed by liquid NMR to determine its purity.

$$(CH_3CH_2O)_3Si - C_6H_6 - Si\,(OCH_2CH_3)_3 + 6\,SOCl_2 \rightleftharpoons$$

$$Cl_3Si - C_6H_6 - Si\,Cl_3 + 6\,SO_2 \uparrow + 6\,CH_3CH_2Cl \uparrow \qquad (Eq.15)$$

2.2.1.3 1,4-Bis(triacetoxysilyl)benzene

1,4-Bis(triacetoxysilyl)benzene was produced similarly to $Si(OAc)_4$ from corresponding chlorosilane (2.061 g, 5.974×10^{-3} mol) and acetic acid anhydride (5.489 g, 0.054 mol, 50 % excess) by slightly modified procedure. The complete acetylation of the chlorosilane was achieved by distilling off $CH_3C(O)Cl$ from the reaction mixture (*Eq.16*). Product was obtained as white crystals and purified by the same procedure as silicone tetraacetate, producing 1.996 g of 1,4-Bis(triacetoxysilyl)benzene (yield: 68.76 %). 1,4-Bis(triacetoxysilyl)benzene was analyzed by liquid NMR to determine its purity.

$$Cl_3Si - C_6H_6 - Si\,Cl_3 + 6\,CH_3C(O)OC(O)CH_3 \rightleftharpoons$$

$$(CH_3(O)CO)_3Si - C_6H_6 - Si\,(OC(O)CH_3)_3 + 6CH_3C(O)Cl \uparrow \qquad (Eq.16)$$

2.2.1.4 Drying of solvents

Solvents were dried by an addition of a drying agent, such as sodium or phosphorous oxide. Sodium was used for toluene and diisopropylether. Dichloromethane reacts violently with sodium and forms possibly dangerous products, therefore in this case phosphorous pentoxide is preferably used. Solvents were distilled and then stocked over molecular sieves in the glovebox.

2.2.2 Synthesis of colloidal suspension

Synthesis were performed under vacuum, dry N_2 or Ar atmosphere using Schlenk techniques and glovebox with a H_2O level below 1 ppm and an O_2 level between 10 and 30 ppm[4]. The glovebox used during this master thesis was the LABster Glove Box Workstation from MBraun.

The gas used in the glovebox passes through a purifier to remove oxygen and water from the inert gas flowing. The typical purifier contains two purification agents. One agent is a molecular sieve that removes water by the process of molecular adsorption. The other agent is called Q5 and is an oxygen reactant material. Oxygen removal from argon, helium, or nitrogen is accomplished with this material that consists of finely divided copper on an alumina support. The copper reacts with oxygen to form coper (II) oxide. In order to avoid leaks as much as possible, the atmosphere inside the glovebox is kept at a higher pressure than the outside air.

Reactions were carried out in autoclaves of 100 ml from TOP Industrie. These autoclaves consist of two pieces: one is the outer stainless-steel part and the other is the inner Teflon part. During the polycondensation step of the synthesis, the solvents with low boiling point tends to evaporate, thus increasing the inner pressure of the autoclave. Therefore, it is necessary to have containers able to resist to high pressures. The autoclave can sustain temperatures up to 250 °C and pressures up to 160 bars.

2.2.2.1 Alkyl halide elimination route

Niobium pentachloride was mixed with part of diisopropylether (0.25 g) in small glass vials to help its dissolution. Then 5 ml of solvent was added and the mixture was left stirring until complete dissolution (ca. 2 days in toluene, 4-5 hours in dichloromethane). In the meantime, silicon tetrachloride was mixed with the rest of diisopropylether (according to the reaction stoichiometry) in 20 ml of solvent in the autoclave. As an example, the pristine catalyst (pure

[4] *N.B.: The point of the synthesis in non-hydrolytic sol-gel process is to avoid by all means the presence of water during the synthesis*

niobium silica inorganic oxide) is shown in (*Eq.17*). In the case of hybrid samples, alkyl- and aryl-chlorosilanes were added to this mixture as well. When niobium pentachloride was completely dissolved, its solution was poured into the autoclave which was then properly closed to avoid any leaks. Following stoichiometric ratios were set for all reactions: Nb/Si = 1/16, Cl/iPr_2O = 2/1. Exact masses of the precursors, solvents used, and other information can be found in (*Table 1*) and (*Table 2*) for each sample.

$$NbCl_5 + \frac{69}{2}\ iPr_2O + 16\ SiCl_4 \rightarrow \frac{1}{2}Nb_2O_5.16\ SiO_2 + 69\ iPrCl \qquad (Eq.17)$$

2.2.2.2 Acetate route

Niobium pentachloride was mixed with diisopropylether (0.25 g) in a small glass vials to help its dissolution. In this case, diisopropylether is used only to dissolve the niobium precursor, but doesn't act as an oxygen donor. Then 5 ml of solvent was added and the mixture was left stirring until complete dissolution (ca. 2 days in toluene, 4-5 hours in dichloromethane). In the meantime, silicon tetraacetate (and alkyl- and arylacetoxysilane in the case of hybrid samples) was dissolved in 20 ml of solvent (*Eq.18*). When clear solutions were achieved in both cases, niobium pentachloride solution was poured into the autoclave which was then properly closed to avoid any leaks. Following stoichiometric ratio was set for all reactions: Nb/Si = 1/16. Exact masses of the precursors, solvents used, and other information can be found in (*Table 1*) and (*Table 2*) for each sample.

$$NbCl_5 + 16\ Si(OAc)_4 \rightarrow \frac{1}{2}Nb_2O_5.16\ SiO_2 + 5\ CH_3COCl + \frac{59}{2}\ C_4H_6O_3 \qquad (Eq.18)$$

Table 1 Stoichiometric ratios, polycondensation and calcination temperature and solvent used for each sample. T=TOL=toluene, A=acetate, DPh=diphenyl, MPh=monophenyl, BPh=bridging-phenylene, MMe=monomethyl

Samples	Silicon precursor	Organosilane precursor	Solvent	Polycondensation temperature [°C]	Calcination temperature [°C]
NbSi-T	16 $SiCl_4$	/	TOL	150	400
NbSi	16 $SiCl_4$	/	CH_2Cl_2	150	400
NbSi-A	16 $Si(OAc)_4$	/	CH_2Cl_2	150	400
NbSi12-4DPh-T	12 $SiCl_4$	4 Ph_2SiCl_2	TOL	150	400
NbSi12-4DPh	12 $SiCl_4$	4 Ph_2SiCl_2	CH_2Cl_2	150	400
NbSi12-4DPh-A	12 $Si(OAc)_4$	4 $Ph_2Si(OAc)_2$	CH_2Cl_2	150	400
NbSi8-8MPh	8 $SiCl_4$	8 $PhSiCl_3$	CH_2Cl_2	150	400
NbSi14-2MPh	14 $SiCl_4$	2 $PhSiCl_3$	CH_2Cl_2	150	400
NbSi14-2MPh-A-T	14 $Si(OAc)_4$	2 $PhSi(OAc)_3$	TOL	200	350
NbSi-8BPh	/	8 $Cl_3Si-Ph-SiCl_3$	CH_2Cl_2	150	400
NbSi12-2BPh	12 $SiCl_4$	2 $Cl_3Si-Ph-SiCl_3$	CH_2Cl_2	150	400
NbSi-8BPh-A-T	/	8 $(OAc)_3Si-Ph-Si(OAc)_3$	TOL	200	350
NbSi8-8MMe	8 $SiCl_4$	8 CH_3SiCl_3	CH_2Cl_2	150	400
NbSi14-2MMe	14 $SiCl_4$	2 CH_3SiCl_3	CH_2Cl_2	150	400

Table 2 Precursors masses weighted for each sample. T=TOL=toluene, A=acetate, DPh=diphenyl, MPh=monophenyl, BPh=bridging-phenylene, MMe=monomethyl

Samples	Mass of Si precursor [g]	Organosilane precursor [g]	Mass of $NbCl_5$ [g]	Mass of iPr_2O [g]
NbSi-T	1.083	/	0.1077	1.432
NbSi	1.081	/	0.1065	1.424
NbSi-A	1.682	/	0.1068	0.2504
NbSi12-4DPh-T	0.8397	0.4323	0.1013	1.237
NbSi12-4DPh	0.8102	0.4034	0.1081	1.248
NbSi12-4DPh-A	1.263	0.4777	0.1085	0.2493

NbSi8-8MPh	0.5202	0.6227	0.1014	1.224
NbSi14-2MPh	0.9384	0.1760	0.107	1.356
NbSi14-2MPh-A-T	1.461	0.2247	0.1106	0.2478
NbSi-8BPh	/	1.037	0.1011	1.125
NbSi12-2BPh	0.9157	0.2727	0.1079	1.326
NbSi-8BPh-A-T	/	1.549	0.1051	0.2475
NbSi8-8MMe*	1.0437	0.9034	0.2081	0.5112
NbSi14-2MMe*	1.9330	0.2502	0.2186	0.5012

* Double batch, the volume of solvent was also doubled

2.2.3 Polycondensation/Gelification

When the autoclaves are properly closed, they are kept in an oven at 150 °C (or 200 °C). All the autoclaves are left in the oven for a week in order to let the polycondensation reactions proceed (*Eq. 8-9*, *11-12*) and the gelification process occur. Autoclaves are then removed from the oven and once they are at room temperature, they are inserted back into the glovebox. The gel which is now formed is then transferred from the autoclaves to Schlenk flasks for the drying step.

2.2.4 Drying of the gel

Gels are dried *in vacuo* overnight at 60 °C using a Schlenk technique, volatiles (solvent and organic products of polycondensation reactions) are collected in a trap kept in liquid nitrogen (-196 °C). Prepared materials are obtained as fine powders after the drying step, collected and stored in the glovebox.

2.2.5 Calcination

Powders are calcined at 350 or 400°C with a Minicor 42 Coreci oven in air flux of 40 ml min^{-1}. The temperature has been programmed to increase by 1 °C min^{-1} for calcination at 350 °C and by 5°C min^{-1} for calcination at 400 °C. The total time of calcination including heating ramp

was 600 min in both cases. The calcination in air has the advantage to help burning the remaining traces of solvent or organic products still adsorbed onto the surface.

2.2.6 Catalytic Reaction + Gas Chromatography

2.2.6.1 Sample preparation

After calcination, samples are sieved in order to obtain particles between 200 and 355 µm. Then, ca. 0.85 g of glass beads is poured inside the reactor (*Figure 7*). After that, 0.192 g of catalyst diluted in 0.65 g of glass beads is added in order to keep the volume of the catalyst bed constant. Finally, the reactor is filled to its top with glass beads. The reactor is a straight fixed bed reactor of 27 cm long with an inner diameter of 0.6 cm, heated by a Minicor 42 Coreci furnace. The heat insulation is ensured by glass wool. Ethanol is delivered into the reactor by a n-300 syringe pump from QiS at the speed of 0.212 g h^{-1} from a 5 ml syringe. The catalyst bed is also flushed with a nitrogen flow of 40 ml min^{-1} delivered by an El-flow mass flow controller from Bronkhorst.

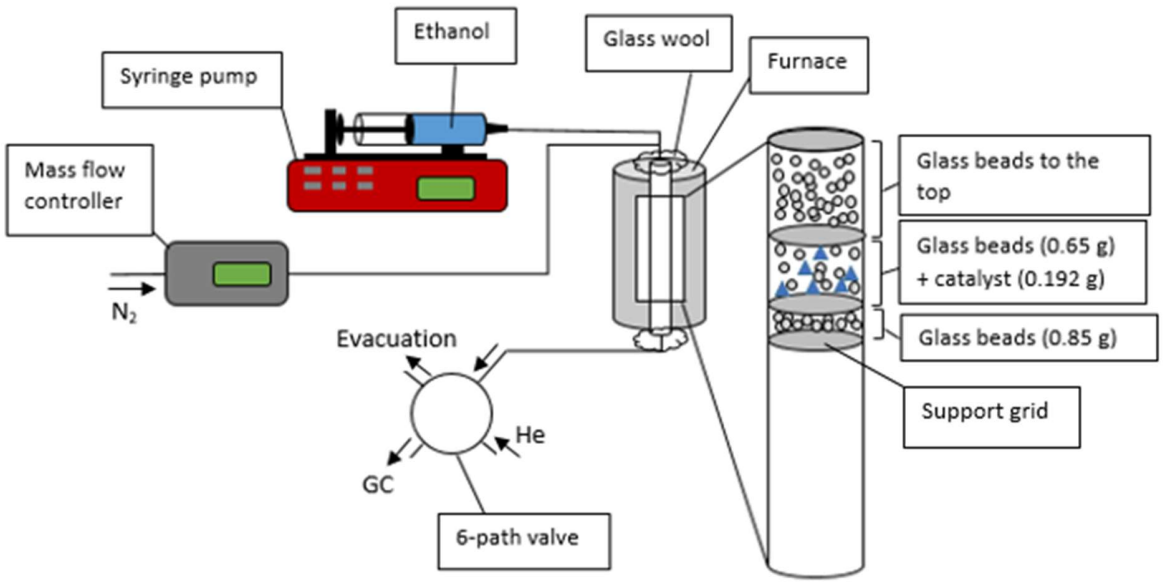

Figure 7 Scheme of catalytic set-up
▲= catalyst particles, o = glass beads

2.2.6.2 Catalysis

The catalytic reaction (*Eq.1-2*) was tested in step mode from 160 °C to 300°C. Some of the samples have been tested at 400°C to see if there was a production of butadiene [39]. For each reaction temperature step, 9 injections were made, at 7 min intervals.

2.2.6.3 Analysis

The products are sent into a 6-path valve connected to a VARIAN 3800 Gas Chromatograph equipped with a flame ionization detector (FID) and a Cydex B capillary column (25 m), with an internal diameter of 0.22 mm and with a film thickness of 0.25 µm. The analysis conditions are:

- Vector gas: Helium
- Pressure at the top of the column: 15 psi
- Injector temperature: 150 °C
- Detector temperature: 250 °C
- Temperature of the column: Kept at 40 °C (no ramp)

2.2.6.4 Calibration

First of all, incoming flows must be calibrated. The syringe pump is calibrated with ethanol so the flow is known (difference between the mass of the syringe + ethanol at the beginning and at the end of pumping time). Then, nitrogen flow and ethylene flow are calibrated with a burette and soap.

Secondly, the GC has to be calibrated as well. The response factors of FID detector to concentration of ethanol and ethylene in N_2 is measured directly (exact concentration can be calculated knowing the flows of all components). Calibration of diethylether is however based on an internal standardization method, which relates to coefficients of relative responses of different compounds. These coefficients are determined using binary mixtures of different concentrations with a reference compound (ethanol). Thus, the relative coefficients are determined using the following equation (*Eq.19*)

$$\frac{A_i}{A_{ref}} = K_{i/ref} \frac{C_i}{C_{ref}} \qquad (Eq.19)$$

Where:

- $K_{i/ref}$ is the relative response coefficient of compound i.
- C_i is the molar concentration of product i in the calibration solution.
- C_{ref} is the molar concentration of the reference in the calibration solution.
- A_i is the area of product i in the calibration solution.
- A_{ref} is the area of the reference in the calibration solution.

2.2.7 Hydrothermal stability in gas phase

A quantity of 192 mg of catalyst particles below 300 µm is weighted, introduced in the reactor, and flushed under nitrogen. The catalyst is mixed with glass beads in the fixed bed reactor in the same way as during the catalysis, and is heated to 250 °C. Distilled water is injected with the syringe pump at the speed of 0.216 g h^{-1}. The liquid water is then vaporized in nitrogen flow of 40 ml min^{-1} before the contact with the catalyst. The water stream (molar ratio: 0.177) and the temperature of 250 °C are then kept for 24 hours.

2.2.8 Characterization techniques

2.2.8.1 Nitrogen physisorption

Nitrogen physisorption is a surface characterization technique which gives textural information such as specific surface area, pore volume, etc. of a catalyst. These textural properties can then be related to the activity of the material.

Theory

Nitrogen adsorption is the method used for the determination of adsorption isotherms of nitrogen at the temperature of liquid nitrogen (-196°C). The principle relies on physisorption, a reversible adsorption phenomenon involving weak and non-specific Van-der-Waals interactions.

The sample is placed in a tube, in which a certain quantity of nitrogen is brought. Once the equilibrium of nitrogen adsorption is reached, the pressure inside the tube is measured. The difference between the starting pressure and the one at equilibrium give access to the actual quantity of adsorbed nitrogen molecules. The adsorption isotherm can then be plotted by repeating this operation at different relative pressures. The relative pressure can be defined as the ratio between the pressure at equilibrium and the one at saturation P_0. The isotherm is thus representing the number of adsorbed nitrogen moles as a function of the relative pressure. The adsorption isotherm is plotted by increasing the P/P_0 ratio to 1, the latter being then progressively decreased to obtain the desorption isotherm.

Surface areas of the samples are determined by the BET method for P/P_0 between 0.05 and 0.35 and the experimental error on the measurement is 10 %. The pore volume (V_p) is representing the volume of nitrogen adsorbed at the maximal relative pressure. Pore diameter was determined by the maxima of the pore distribution curve obtained by the Barett-Joyner-Halenda (BJH) method measurement during desorption.

Method

The nitrogen physisorption experiments were carried out on a Micromeretics TriStar 3000, and the data were displayed and handled on the associated software (TriStar 3000 V6.01). Regarding the sample preparation, between 50 and 100 mg is weighted and placed into the quartz tubes. They are then degassed for ca. 10 hours at 150°C under vacuum.

2.2.6.3 X-ray photoelectron spectrometry (XPS)

XPS is a surface characterization technique that measures the electronic state of the atoms on the analyzed surface.

Theory

The principle of this method is the irradiation of a material with an X-ray beam with a fixed wavelength (monochromatic), which cause a loss of electrons from the atoms of a depth from 0 to 10 nm. Such electrons are called photoelectrons and are collected and then analyzed in a

detector. Each element has photoelectrons with a distinct energy, thus the analysis of photoelectrons can tell us about the chemical composition of the surface. The binding electron energy (specific for each element) can be determined by using the following energy conservation equation (*Eq.20*):

$$h\nu = E_k + E_b + E_c + \Phi \qquad (Eq.20)$$

Since the energy of a monochromatic X-ray beam ($h\nu$) is known (Al: K_α X-rays, $h\nu$= 1486.7 eV), the electrons kinetic energies (E_k) are measured and since the work function (Φ) and the interaction energy between the surface and the electrons (E_c) are known and constant, the binding energy (E_b) can be determined with a precision of about 0.2 eV.

Method

Analysis were carried out on an SSX 100/206 photoelectrons spectrometer from Surface Science Instruments (USA) equipped with an Al RX monochromatic and micro-focused source. Samples were pressed in small cups with a diameter of 4 mm and disposed on a conducting carousel sample carrier made of aluminum. The pressure inside the analysis chamber is about 10^{-6} Pa. The angle between the normal to the surface and the axis of the input lens of the analyzer was 55°. The analyzed zone was approximately 1.4 mm² and the pass energy was fixed at 150 eV. Under these conditions, the half-height width (FWHM) of the Au $4f_{7/2}$ photo-peak measured on a standard cleaned gold sample was about 1.6 eV. An electron gun set at 8 eV and a nickel grid placed 3 mm above the surface of the sample were used to stabilize the charge.

The C-(C,H) component of the C_{1s} peak of carbon was set at 284,8 eV to set the scale of the binding energy. The data processing was carried out with the CasaXPS program (Casa Software Ltd, UK). Some spectra were decomposed by the program (using the least-squares method adjustment) with a Gaussian and Lorentzian function product model after subtraction of a nonlinear baseline. The molar fractions were calculated using standard peak areas based on the acquisition parameters and sensitivity factors provided by the manufacturer.

2.2.6.4 Thermogravimetric analysis (TGA)

Thermogravimetric analysis is a technique in which the mass of a substance is monitored as a function of temperature or time as the sample is submitted to a controlled temperature program in a controlled atmosphere.

Theory

The TGA consists of a precision balance with a sample pan located outside a furnace with a programmable control temperature. The samples are set into small ceramic crucibles which are placed on the pan and a robot will take samples one by one and place them inside the furnace. The temperature is generally increased at constant rate. Various thermal reaction can happen depending on the atmosphere present in the analysis chamber. Air is used, for example, when the point is to quantify the amount of an organic specie incorporated into a hybrid sample. The air will thus completely burn the organic moieties in a certain range of temperature, leaving the substrate that is thermally resistant (e.g. inorganic oxide).

Method

The measurements were carried out in 70 µL alumina crucibles which contained ca. 15 mg of the sample. Beforehand, crucibles were washed with acetone and were passed under oxidizing flame. During the measurement, samples were flushed with dry air with a speed of 50 ml min^{-1}. The temperature profile is linear and goes from 30 °C to 1000 °C, at 5 °C min^{-1}. The apparatus used was a TGA/SDTA-851e Mettler Toledo equipment.

2.2.6.5 Infrared spectroscopy (IR)

Infrared spectroscopy is a commonly used method of identifying chemical compounds in both organic and inorganic chemistry. It can be used on gaseous, liquid or solid samples. It has various applications including chemical analysis, forensic analysis, environmental impurities detection, etc.

Theory

The infrared domain has wavelengths from 0.75 µm to 1000 µm and is located beyond red in the visible spectrum. The energy coming from IR radiations is sufficient to change molecular vibration energy but cannot induce electronic transitions. Infrared spectroscopy is a measurement of the decrease in the intensity of the radiation in function of its wavelength that passes through a sample. This technique is mainly used for qualitative analysis because it allows one to see the type of bond between atoms (moieties and chemical functions). Since the Lambert-Beer law is verified in infrared, the IR spectroscopy can be used also as a quantitative method. Indeed, infrared spectrum display a transmission (intensity fraction transmitted compared to the initial intensity) expressed in a percentage as a function of the wave number (*Eq.21*):

$$\mathrm{A} = \log\left(\frac{1}{\mathrm{T}}\right) \qquad (Eq.21)$$

Where:

- A is the absorbance at a given wavelength.
- $\mathrm{T} = \frac{\mathrm{I}}{\mathrm{I}_0}$ is the transmittance which is the ratio between the intensity of the incident light and the intensity of the outgoing light.

Method

Pellets are prepared by grinding ca. 2 mg of sample with 150 mg of purified KBr (to remove scattering effects from big crystals). The powder mixture is then pressed in a mechanical press from SPECAC to form a translucent pellet through which the beam of the spectrometer can pass. Measurements have been carried out on an EQUINOX 55 Bruker spectrometer, and the program used to record the data was OPUS.

2.2.6.6 Nuclear Magnetic Resonance spectroscopy (NMR)

Nuclear magnetic resonance spectroscopy is a low energy analytical technique that exploits the property of certain nuclei to possess a nuclear magnetic moment. Nuclei of atoms are probed so we can obtain information about the environment and the connectivity of these atoms inside a molecule (2D and 3D structure).

Theory

Like the electron, the proton and the neutron have an intrinsic angular moment. This angular momentum is characterized by the spin quantum number (i). For electrons, protons and neutrons, i=±½. Within the nucleus, protons and neutrons pair with each other (+ ½ with -½).The quantum number of total spin (i_{total}) of a nucleus therefore depends on the number of unpaired protons and neutrons. Only nuclei in which $i_{total} \neq 0$ are observed in NMR. Isotopes of particular interest are ^{1}H, ^{13}C, ^{19}F, ^{29}Si and ^{31}P, all of which have i=½. Since the analysis of this spin state is fairly straightforward and taking into account the elements investigated in this study, the NMR spectroscopy will be limited to ^{1}H, ^{13}C and ^{29}Si.

Liquid NMR method

As a part of this project, liquid NMR was applied to analyze the purity of the synthesized 1,4-Bis(triacetoxysilyl)benzene and 1,4-Bis(trichlorosilyl)benzene. Solution NMR spectra were recorded on a Bruker Avance II 300 equipped with a BBO 5 mm NMR probe z-gradient coil and a B-ACS-60 autosampler. It operates at 299.80 MHz for ^{1}H and at 75.38 MHz for ^{13}C with deuterated solvents as the external lock. The ^{1}H and ^{13}C $\{^{1}H\}$ NMR spectra were referenced to the residual proton signals or carbon resonances of benzene-d6 (7.15 and 128.0 ppm, respectively) and $CDCl_3$ (7.20 and 77.0 ppm).

Solid-state NMR method

Solid-state NMR was performed on catalyst powders. Solid-state ^{13}C and ^{29}Si (CP)MAS NMR spectra were acquired on a Bruker 500 MHz NMR spectrometer. Samples were loaded into 4 mm zirconia rotors and stoppered with teflon plugs. Magic angle spinning rates were 8 kHz for ^{29}Si and ^{13}C CPMAS. Chemical shifts were referenced externally to ^{29}Si δ[5] [3-(trimethylsilyl)-1propanesulfonate]: 0.00 ppm; ^{13}C δ [adamantane]: 38.68 ppm.

2.2.6.7 Ammonia Temperature Programmed Desorption (NH_3-TPD)

Temperature programmed desorption allows to follow the desorption of a probe molecules from a sample as its temperature increase.

Theory

In the same way as the nitrogen adsorption, molecules which come in contact with a surface adsorb onto it to minimize their interfacial energy with the surface. This interaction is characterized by a specific binding energy which depends on the combination of the adsorbate and the surface. If the surface is heated, the energy provided by the increasing temperature is transferred to the adsorbed species, causing the breaking of the bond and molecules will desorb. The temperature at which this phenomena occurs is called the desorption temperature. Here the adsorbate studied is the NH_3 as it is a basic molecule which will adsorb onto acidic sites of the catalyst. By quantifying the amount of NH_3 desorbed from the sample and by looking at the desorption temperature, one can estimate the number of acidic sites on the surface of the catalyst and the strength of these sites respectively.

[5] δ = chemical shift

Method

The NH_3 temperature programmed desorption (NH_3-TPD) was performed with a Hiden CATLAB-PCS combined microreactor and mass spectrometer (MS) system, the MS being equipped with a quadrupole. Around 50 mg of sample is weighted in a quartz tube, which is then put in the microreactor. The temperature followed the program described in (*Figure 8*).

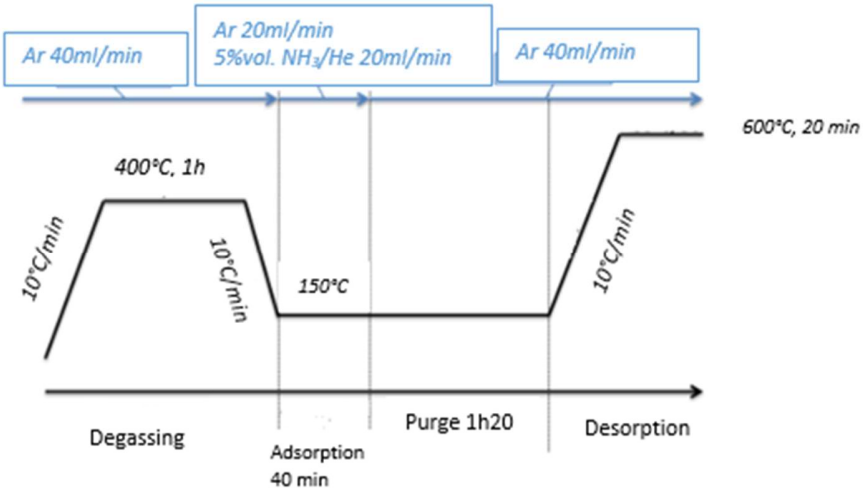

Figure 8 NH_3-TPD temperature program

The specific masses analyzed by the mass spectrometer were 17 (Ammonia), 40 (Argon), 28 (Nitrogen), 18 (Water), 4 (Helium). The analysis of m/z = 78 (C_6H_6) was also chosen for phenylated samples, as it could be helpful to determine the thermal resistance of incorporated phenyl groups.

3. Results and discussion

In this chapter, a first part will detail the physicochemical characteristics of the synthesized materials. In a second step, the catalytic results will be shown and discussed in relation to the properties of each sample. Finally, the last part will be dedicated to the stability of samples under specific conditions.

3.1 Textural properties

Textural properties of each sample are displayed in *Table 3*. These results are obtained from the nitrogen physisorption isotherms by the BET method for the specific surface area, and by measurements of the pore volume. The pore diameter was calculated by the BJH method applied the desorption part of the isotherms.

Table 3 Textural properties of synthesized samples

Sample	Specific surface area (SSA) [$m^2\ g^{-1}$]	Pore volume (PV) [$cm^3\ g^{-1}$]	Pore size (PS) [nm]
NbSi-T	830	2.59	11.6
NbSi	690	1.29	5.04
NbSi-A	700	0.266	2.58
NbSi12-4DPh	600	1.24	8.79
NbSi12-4DPh-A	910	0.614	2.90
NbSi8-8MPh	610	0.397	3.06
NbSi14-2MPh	630	0.587	4.04
NbSi14-2MPh-A-T	720	1.12	6.29
NbSi-8BPh	1030	1.62	6.89
NbSi12-2BPh	660	0.604	3.78
NbSi-8BPh-A-T	670	0.875	6.91
NbSi8-8MMe	690	2.27	13.1
NbSi14-2MMe	770	1.27	6.57

The first important ascertainment that comes out of these results is that all these samples are mesoporous (pore diameter between 2 and 50 nm) even though **NbSi-A** has relatively small mesopores close to the microporosity (<2 nm). Isotherm of this sample is reported in *Figure 9*. The shape of this isotherm is actually in between type 1 and type 4, showing also a H4 hysteresis loop [40], which is often associated to narrow slit pores [41]. The analysis of the t-plot stated that 44 % of the pore volume is attributed to micropores.

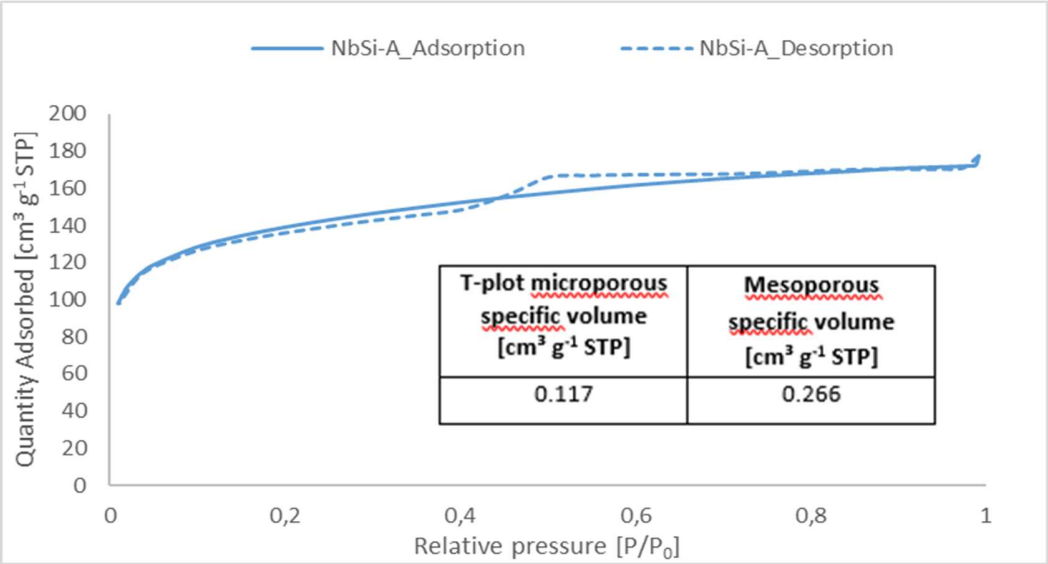

Figure 9 Isotherms of sample NbSi-A measured by nitrogen physisorption

Although sample **NbSi-A** show some microporous characteristics, all other samples are exclusively mesoporous and possess type 4 isotherms with a hysteresis. To illustrate this, isotherms of samples **NbSi**, **NbSi-8BPh** and **NbSi8-8MMe** are pictured in *Figure 10*.

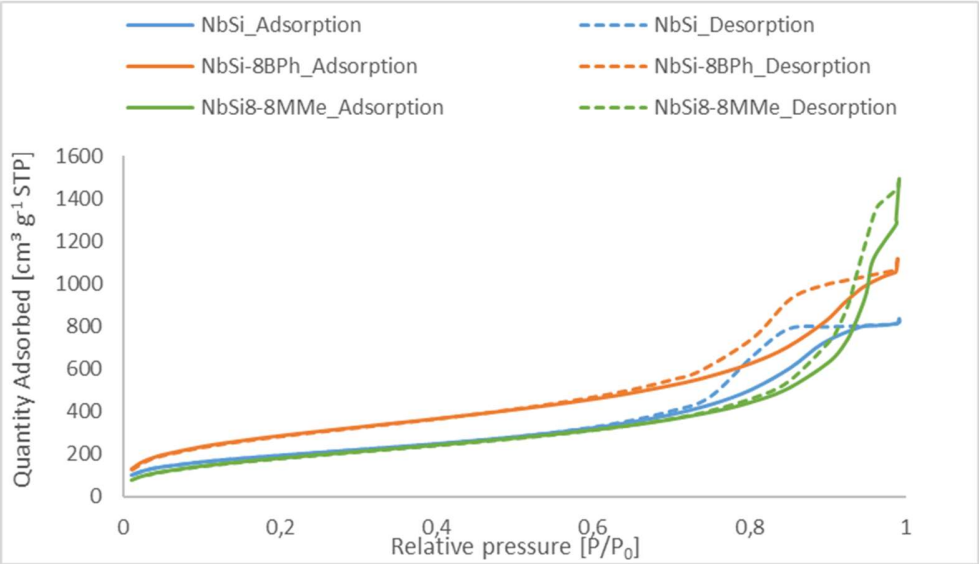

Figure 10 Isotherms of sample NbSi, NbSi-8BPh and NbSi8-8MMe measured by nitrogen physisorption

The mesoporous nature of these samples is expected as it is one of the consequences of the non-hydrolytic sol-gel process. It makes it possible to overcome the diffusion constraints and possible non-accessibility of the active sites.

Silica-alumina catalyst support, grade 135 (from Sigma-Aldrich), which is used as a reference sample for the dehydration of ethanol, shows a SSA of 600 $m^2\ g^{-1}$, a pore volume of 0.732 $cm^3\ g^{-1}$ and a pore size of 4.17 nm. The specific surface areas obtained through NHSG are in most cases significantly higher than the one of the reference sample.

Regarding the impact of the introduction of organic groups inside the framework of the niobium silica, it seems that higher organic content increases the pore volume and pore diameter with two exceptions (**NbSi8-8MPh** and **NbSi12-4DPh-A**). The small impact of their high organic content on the textural properties could signify that the actual incorporation of organic groups is worse than expected. This hypothesis was later verified by thermogravimetric analysis (*c.f.: 3.4.3*). Samples from acetate route also display a similar trend. Apart from, the microporosity of **NbSi-A**, no clear difference in textural properties stands out.

3.2 Acidity

Literature has established an existence of a correlation between the catalyst acidity and the catalytic activity. The Lewis acidity is generally attributed to the surface-exposed coordinatively-unsaturated Nb^{5+} sites. With low amount of niobium (<10 %), Nb_2O_5-SiO_2 possesses mainly Lewis acid sites (*Figure 3*). Since the ethanol dehydration requires acid catalysis, a study on the acidity of the synthesized samples was performed by NH_3-TPD (*Table 4*).

Table 4 NH_3-TPD of synthesized samples

Sample	Acid sites [mol g^{-1}]	Acid sites [µmol m^{-2}]
NbSi-T	/	/
NbSi	2.42E-04	3.49E-01
NbSi-A	7.68E-05	1.10E-01
NbSi12-4DPh-T	/	/
NbSi12-4DPh	2.34E-05	3.94E-02
NbSi12-4DPh-A	/	/
NbSi8-8MPh	1.14E-04	1.86E-01
NbSi14-2MPh	2.43E-04	3.85E-01
NbSi14-2MPh-A-T	2.34E-04	3.25E-01
NbSi-8BPh	1.72E-05	1.66E-02
NbSi12-2BPh	2.54E-04	3.84E-01
NbSi-8BPh-A-T	1.43E-04	2.13E-01
NbSi8-8MMe	1.53E-04	2.23E-01
NbSi14-2MMe	1.06E-04	1.37E-01

Inorganic and hybrid samples were analyzed in order to study the effect of the incorporation of organic groups on the acidity of the catalyst. A general statement is that all samples present more or less the same number of acid sites (from 7.68E-05 mol g^{-1} for **NbSi-A** to 2.54E-04 mol g^{-1} for **NbSi12-2BPh**), except for samples **NbSi12-4DPh** and **NbSi-8BPh**, which show significantly lower acidity (respectively 2.34E-05 and 1.72E-05 mol g^{-1})**.**

To dress the complete portrait of the acidity, along with the number of acid sites, the strength has to be also investigated. The strength of the acid site can be evaluated by the temperature at which the ammonia molecules desorb from the acid sites. TPD profiles of some samples are presented in *Figure* 11, in which the acidities of alkyl halide elimination and acetate route samples are compared.

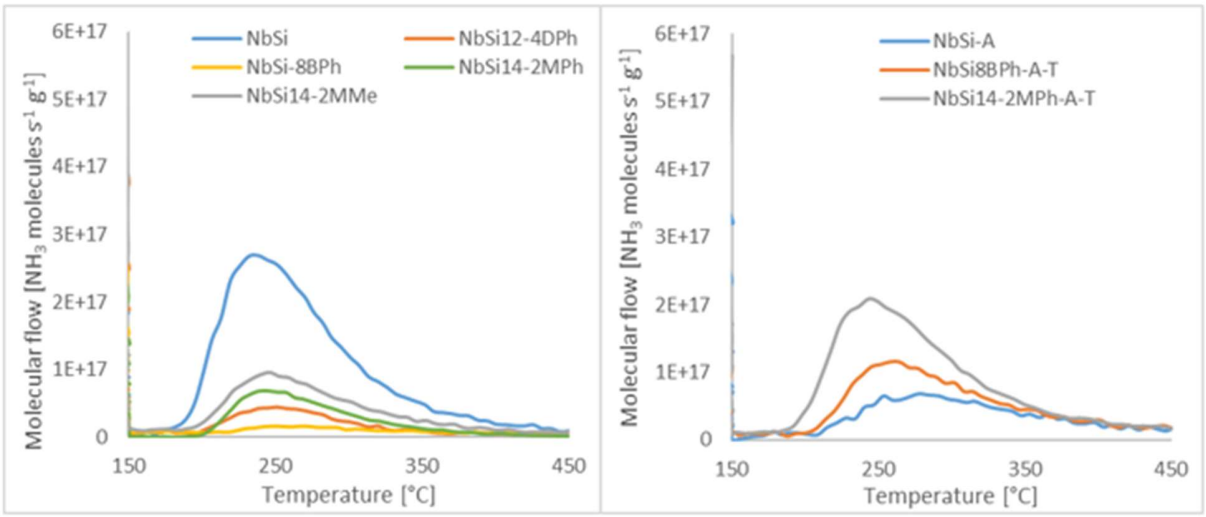

Figure 11 Strength of acid sites in different samples, alkyl halide vs. acetate route

First of all, *Figure* 11 displays a different behavior between the two different synthetic routes. In samples from the alkyl halide route, more organic content decreases systematically the acidity of the sample whereas it is the opposite in the sample synthesized by the acetate route. Indeed, acetate samples have an increased acidity when the organic content is higher. This could be attributed to the lower reaction rates of organosilane precursors with respect to silicon precursors. In the case of the alkyl halide route, a less reactive organosilane precursor will lead to the chloro-alkoxy-niobium intermediate reacting more readily with niobium precursors ($NbCl_5$). As it is known that the main acid sites are Lewis acid sites coming from NbO_4 species (*Figure 3*) only exist in well dispersed niobium materials, lower dispersion of niobium would imply less Lewis acid sites. In the case of the acetate route, the niobium precursor cannot react with itself. Thus, if the reaction rate between the organosilane precursors is decreased, it would gave more time to the $NbCl_5$ to react with organosilanes compounds, which would improve the dispersion of the

niobium species. Along with the previous hypothesis, a higher dispersion would also increase the number of Lewis acid sites (NbO_4).

Samples synthesized by the alkyl halide elimination pathway do not display any shift in the peak related to the incorporation of organic groups. However, the width of the peaks is slightly different in the case of the pristine sample. Indeed, the desorption of ammonia begin at a lower temperature in comparison to the hybrids samples. This could mean that the distribution of acid sites is slightly different in the case of samples without organic groups, meaning that the hybridization can induce a loss of a particular acid sites, which are actually the weakest acid sites.

The strength of acid sites is in the same temperature range for both synthetic routes, however the acetate sample has a different trend than the alkyl halide samples. The incorporation of phenyl groups inside the framework engenders a shift to lower temperature, meaning that phenyl moieties weaken the overall strength of acidity in the samples. Nevertheless, no clear trend based on the type or amount of organic groups incorporated can be highlighted.

Pyridine adsorption should be considered as an additional technique to confirm that the hybridization does not change the type of acid sites of the Nb_2O_5-SiO_2 mixed-oxides.

3.3 Homogeneity of the mixed-oxide

It is known that the homogeneity the Nb_2O_5-SiO_2 has an impact on the nature of the acid sites and the catalytic performances [27], therefore it is important to characterize the incorporation of the niobium atoms inside the hybridized silica framework. To analyze the loading of Nb inside the framework of the synthesized samples, two different techniques have been performed: (i) Infrared spectroscopy and (ii) XPS.

3.3.1 Characterization of incorporated Nb by IR

Infrared spectroscopy is a method of analysis based on the absorption of infrared radiation by the material. It allows, through the detection of the characteristic vibrations of the chemical bonds, to carry out the analysis of the chemical functions present in the materials. The study of asymmetric elongation vibrations of Si−O−Si bridges and Si−O−M bridges of mixed-oxides

compared to each other makes it possible to differentiate respective degrees of homogeneity of the samples [42].

Silica usually displays two peaks related to the Si−O−Si bridges: One of higher intensity at 1100 cm^{-1} corresponding to the asymmetrical stretching of Si−O−Si bridges and the other at 800 cm^{-1} related to the symmetrical stretching [43].

Besides, another important band has been observed at around 960 cm^{-1} in metal-containing mixed-oxides by the literature [44,45] which is absent in the spectra of pure silica. This band has also been observed in different oxides containing framework metals and has been attributed to ν_{as} Si−O(−M). Although its origin is still under discussion, it is generally taken as an indication of metal incorporation into the framework of the material. Mixed-oxides of Nb_2O_5-SiO_2 analyzed by IR reported in the literature exhibit this band between 930 and 970 cm^{-1} [46]. *Figure 13, Figure 12* and *Figure 14* display a band in this range of vibration (960 cm^{-1}). These figures also show a second peak that can be attributed to the asymmetrical elongation of Si−O−Si bridges at 1080 cm^{-1}. This peak is normalized to allow for the identification of the niobium incorporation degree.

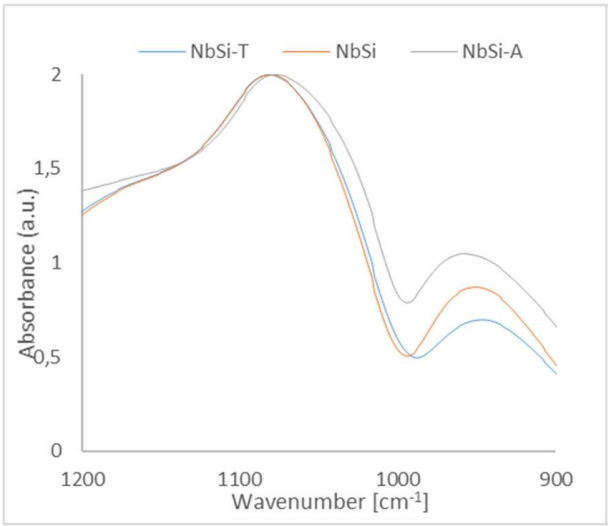

Figure 12 Absorbance of pristine samples

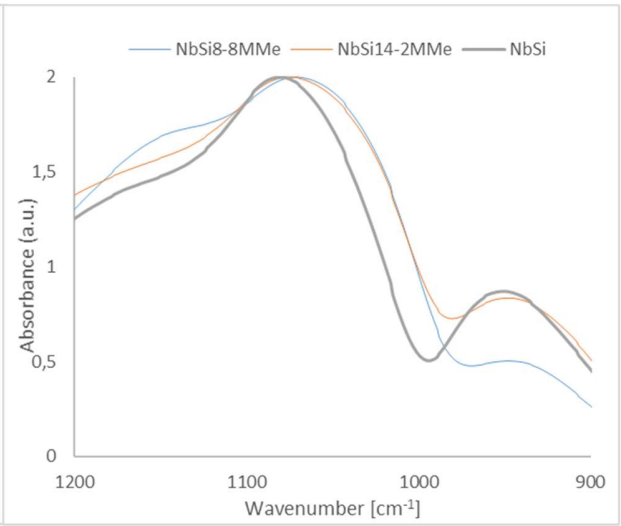

Figure 13 Absorbance of methylated samples

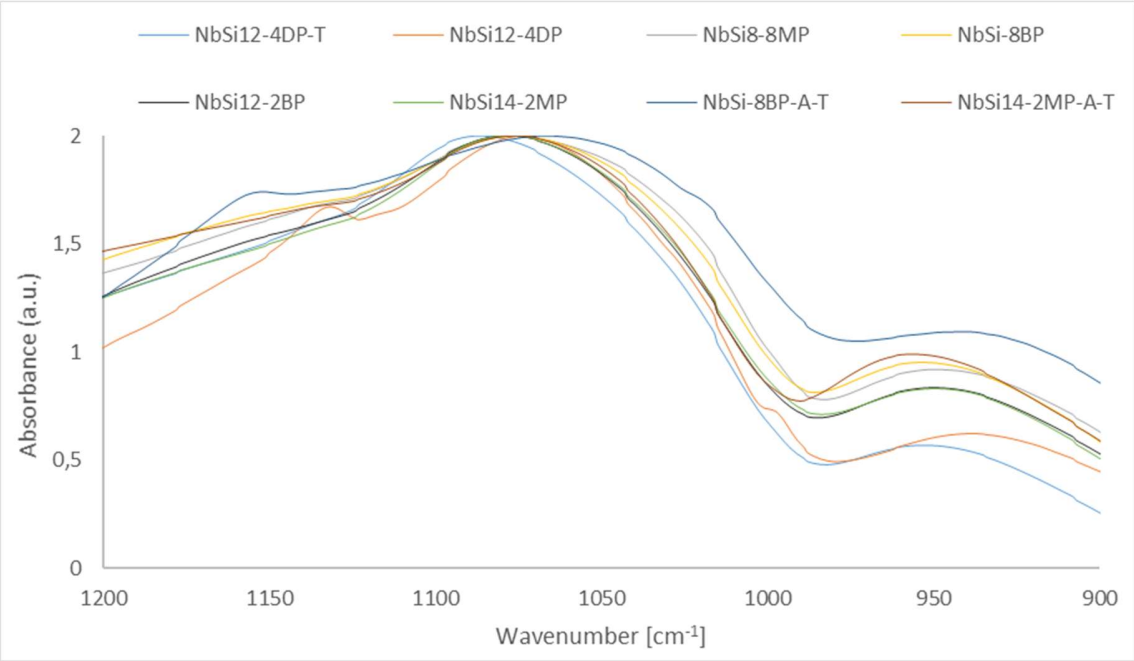

Figure 14 Absorbance of phenylated samples

First of all, *Figure 12* exhibits a difference in the intensity of the band at 940-970 cm^{-1} corresponding to ν_{as} Si−O(−Nb) between the non-hybridized samples. Acetate samples display the highest intensity for peaks corresponding to amount of Si−O−Nb bridges. This proves again that the Nb dispersion is higher in the acetate route than in the alkyl halide route. This difference can be interpreted by the existence of the chloro-alkoxy-niobium intermediate in the alkyl halide route. As this intermediate can either react with silicon or niobium precursor and this condensation step is controlled by reaction rates (niobium intermediate + niobium precursor vs. niobium intermediate + silicon precursors), the dispersion of Nb in the framework could be worse than in the other synthetic route (*c.f.: 1.4.2*), thus yielding a material containing less Nb−O−Si bridges. Indeed, the acetate route does not involve any intermediate and the niobium precursors can only react with silicon precursors, which improves the dispersion of niobium species.

Secondly, niobium dispersion is lower when toluene is used as a solvent in alkyl halide elimination. As a matter of fact, this could be a consequence of the synthesis procedure, mainly the time it takes to dissolve $NbCl_5$ (niobium precursor for both synthetic routes) in the solvent. It requires two to three days for the $NbCl_5$ to dissolve in toluene whereas it only takes few hours for this precursor to dissolve in dichloromethane. As it is hard to obtain a clear and homogeneous

solution of Nb precursor in toluene, the mixing with silanes precursors can happen before complete dissolution of $NbCl_5$ which leads to loss of niobium species. As a consequence of this, lower incorporations of niobium in samples prepared in this solvent are recorded.

Figure 13 displays IR spectra of two samples with different loadings of methyl groups (**NbSi8-8MMe** and **NbSi14-2MMe**). Sample with lower content of methyl groups clearly shows higher content of supposed Si−O−Nb bridges. The methyl-silicon precursor probably has a different reaction rate constant for the condensation reaction. Since these two samples were made through the alkyl halide elimination route (*Eq.8-10*), the chloro-alkoxy-niobium intermediate has now the choice to react with Nb chlorides, Si chlorides or Si-methylated chloride. If the reaction rates is significantly lower between niobium species and methylchlorosilanes, the chloro-alkoxy-niobium will be more likely to react with Nb chlorides, yielding a less homogeneous material. This explanation means that the higher methyl content the less Nb gets dispersed.

The purpose of *Figure 14* is to show the differences in the absorbance between different phenylated samples according to the organic group loading and the preparation method. Two interesting observations can be made out of this figure. First, samples from acetate route display a higher proportion of Si−O−Nb bridges. Similar behavior was observed in the case of pristine samples (**NbSi** vs. **NbSi-A**) confirming that the acetate route is generally showing higher niobium dispersion.

On the other hand, diphenylated samples seem to have the worst niobium incorporation out. This could explain why the acidity of sample **NbSi12-4DPh** is lower. Indeed, we know that the main acid sites of the Nb_2O_5-SiO_2 sample are the Lewis acid sites coming from NbO_4 species (*Figure 3*) that exist only in the case of well dispersed Nb species. Since **NbSi12-4DPh** exhibit less Si−O−Nb bridges, there are probably less NbO_4 species, meaning less acidity as a consequence. However, this hypothesis only covers **NbSi12-4DPh** but not **NbSi-8BPh** which also has a lower acidity, but with a higher content of Si−O−Nb bridges.

3.3.2 Characterization of incorporated Nb by XPS

Knowledge of the location and coordination of the transition metals cations in the network of the structure is of importance as it could help understanding the performance and mechanisms of catalytic reactions. XPS provides information about the chemical composition of the surface of materials. This technique will be useful to compare to infrared spectra, as niobium atoms content will be exposed here whereas infrared display oxo-Nb−Si bridges. This will be helpful for the determination of the nature of Nb species.

The Nb(3d) photoelectron peak is used to measure the concentration of Nb at the surface of the sample. This peak is deconvoluted in a doublet corresponding to of the Nb($3d_{3/2}$) and Nb($3d_{5/2}$) photoelectron peaks [47]. The difference between the binding energy of Nb($3d_{3/2}$) and Nb($3d_{5/2}$) is fixed at 2.6 eV [47]. The Nb($3d_{5/2}$) obtain peak is systematically situated in the 208.1-208.5 eV range. This value could correspond to Nb^{5+} oxidation state, even if it differs from that of bulk Nb_2O_5 (207.1 eV) [48]. An explanation on the higher binding energy of the Nb($3d_{5/2}$) peak of Nb_2O_5-SiO_2 mixed-oxide than the Nb_2O_5 can be made. The Pauling electronegativity of each element is different, as niobium has 1.6 while silicon has 1.9. Since the silicon is more electronegative than niobium, the electron density will be lower around the niobium present as isolated species in the silica matrix. Thus, the binding energy of the remaining electrons will increase. Analyses of the IR spectra show that samples with higher dispersion of niobium are actually the ones that have the highest shift in the binding energy.

This hypothesis is also confirmed by the shoulder in the asymmetrical O(1s) peak corresponding to Si−O−Nb bridges, where the binding energy is lower because one of the two silicon atom has been replaced by a niobium atom which is less electronegative. As a consequence, the electron density around the oxygen is higher and the binding energy of the electrons decrease. The asymmetry of the O(1s) photoelectron peak (533 eV) suggests indeed the presence of Nb−O−Si bonds, which can testify the good dispersion of the niobium species into the framework. An example of this feature is presented in *Figure 15* in the analysis of O(1s) peak of sample **NbSi14-2MPh-A-T**. As an insight of the niobium dispersion can be extracted from this feature, the appearance of this asymmetry according to the sample is reported in *Table 5*. Sample

NbSi-8BPh and **NbSi8-8MMe** are the only samples in which the asymmetry of the O(1s) peak is not present. The low amount of Si−O−Nb bridges discovered in infrared analysis of sample **NbSi8-8MMe** supports the fact that the incorporation of relatively high amount of methyl groups is inversely proportional to the dispersion of niobium. However, infrared spectrum of **NbSi-8BPh** show a relatively high content of Si−O−Nb bridges but no asymmetry is found in XPS. The reason behind this different result could be that the surface composition is thoroughly different from bulk composition (see below discussion on Si/Nb ratios). A high degree of Si−O−Nb bridges does not automatically imply that they are well distributed inside the whole framework. In this case, a relatively high amount of Si−O−Nb bridges can be found in the bulk of the material, but the surface does not show the same trend. Since the catalytic reactions take place on the surface, a smaller amount of niobium well dispersed at the surface could affect the catalytic properties of this sample.

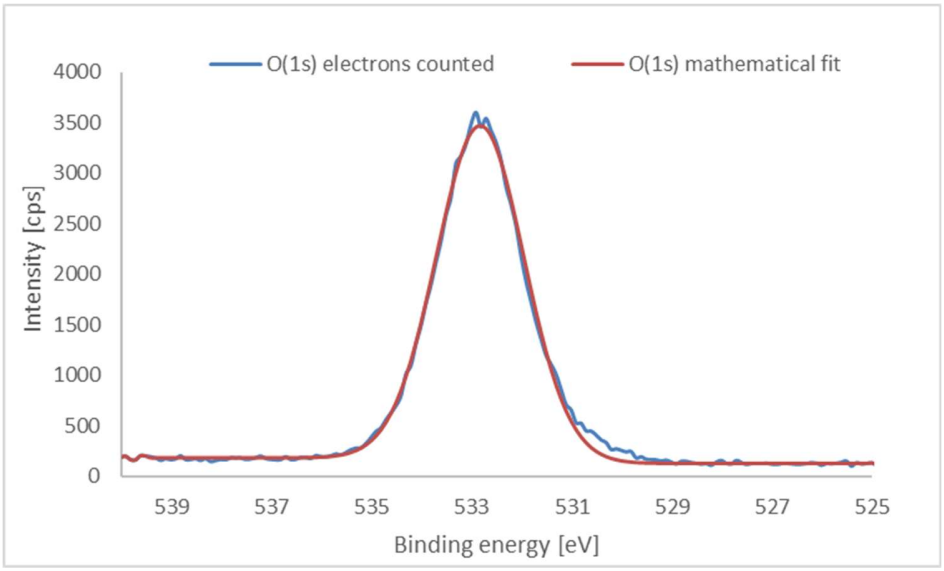

Figure 15 Asymmetry in O(1s) peak of sample NbSi14-2MPh-A-T in XPS

The content of Nb at the surface of the silica framework can be evaluated by reporting the calculated silicon atomic concentration to the niobium one. The different ratios are displayed in *Table 5*. As a reminder, all the syntheses were set to reach a ratio of silicon to niobium of 16 to 1.

Table 5 XPS Results. Ratios of silicon to niobium inside the framework

Sample	Ratio Si/Nb (expected: 16)	Position of Nb($3d_{5/2}$) peak [eV]	Asymmetry of O(1s) peak	Aromatic shake-up
NbSi-T	54	208.1	+	-
NbSi	19	208.3	+	-
NbSi-A	25	208.3	+	-
NbSi12-4DPh-T	58	208.3	/	+
NbSi12-4DPh	20	208.4	+	+
NbSi12-4DPh-A	76	208.2	+	+
NbSi8-8MPh	21	208.5	/	-
NbSi14-2MPh	20	208.3	+	-
NbSi14-2MPh-A-T	23	208.5	+	-
NbSi-8BPh	43	208.4	-	+
NbSi-8BPh-A-T	25	208.5	+	+
NbSi8-8MMe	25	208.3	-	-
NbSi14-2MMe	22	208.5	+	-

Whereas infrared spectra and analysis of the asymmetrical O(1s) peak in XPS gives information on the amount of Si−O−Nb bridges, ratios of niobium to silicon exhibit directly the actual niobium content at the surface. For all synthesized samples, the desired ratio (Si/Nb=16) is not reached. The usual ratio present at the surface varies between 19 (**NbSi**) and 25 (**NbSi-A**) and this slight increase of Si/Nb ratio can be explained by loss of niobium precursor during its manipulation (weighting, dissolution, mixing). Occasionally, the amount of Nb at the surface is really low, as it is the case for **NbSi-T, NbSi12-4DPh-T**, **NbSi12-4DPh-A** and **NbSi-8BPh** and those samples will be discussed in more detail**.**

NbSi12-4DPh-T and **NbSi12-4DPh-A** contain the lowest amount of niobium at the surface among all the samples. Even though the same sample of same composition synthesized by the alkyl halide elimination route in CH_2Cl_2 (**NbSi12-4DPh**) shows a regular amount of niobium, it seems that the incorporation of this type of organic moieties has harmful consequences on the niobium incorporation. The identical conclusion was drawn on the basis of IR spectra analyses.

The lack of **NbSi-8BPh** O(1s) peak asymmetry was already discussed, but in addition to that the actual niobium concentration at the surface is really low. This could explain why, actually, the asymmetry of the O(1s) peak is not perceivable, as low niobium amount at the surface automatically signifies a low amount of Si−O−Nb bridges. Nonetheless, **NbSi-8BPh** has poor surface properties and that should be taking into account for the following catalytic tests. It should be noted that this conclusion is in good agreement with the results of NH_3-TPD, where only low amount of acid sites was found in this sample.

Further investigation on the existence of the aromatic shake-up can be considered. This characteristic broad peak only appears in the samples with the highest content of phenyl moieties confirming their successful incorporation into the structure of hybrid samples. The only exception is sample **NbSi8-8MPh**, which does not display the aromatic shake-up, despite the high amount of organosilane precursors that was added during the preparation. It is probably due to significantly worse incorporation of organic groups than expected, which was already suggested (*c.f.: 3.1*).

3.4 Incorporation of the organic groups

Several methods have been used to characterize and quantify the incorporation of the organic moieties inside the hybrids: (i) IR, (ii) TPD, (iii) Solid-state NMR and (iv) TGA.

3.4.1 Infrared spectroscopy

Infrared spectroscopy can reveal absorption bands of vibrations of organic groups in organic-inorganic hybrids materials. Many reports that give data on the infrared bands of organosilicon materials have been elaborated [49].

Phenyl-silicon moieties in polysiloxane can be easily identified by the 1430 cm^{-1} band corresponding to C−C stretching vibration of aromatic rings. Aside from this band, there are two strong bands, at 710 and 700 cm^{-1}, of approximately equal intensity. These two bands correspond

to C−H bending in aromatic rings. The diphenyl-silicon samples also usually have few bands in the 740-700 cm^{-1} region. The Si−CH_3 group in silica is easily recognized by a strong, sharp band at about 1270 cm^{-1} together with one or more strong bands in the range of 780-760 cm^{-1}. Last but not least, when it comes to methyl and phenyl incorporation, one should observe the C−H stretching band at 3150-3000 cm^{-1} for aromatic and at 3000-2850 cm^{-1} for aliphatic species. All spectra of the analyzed samples are shown in *Figure 16, Figure 17* and *Figure 18*.

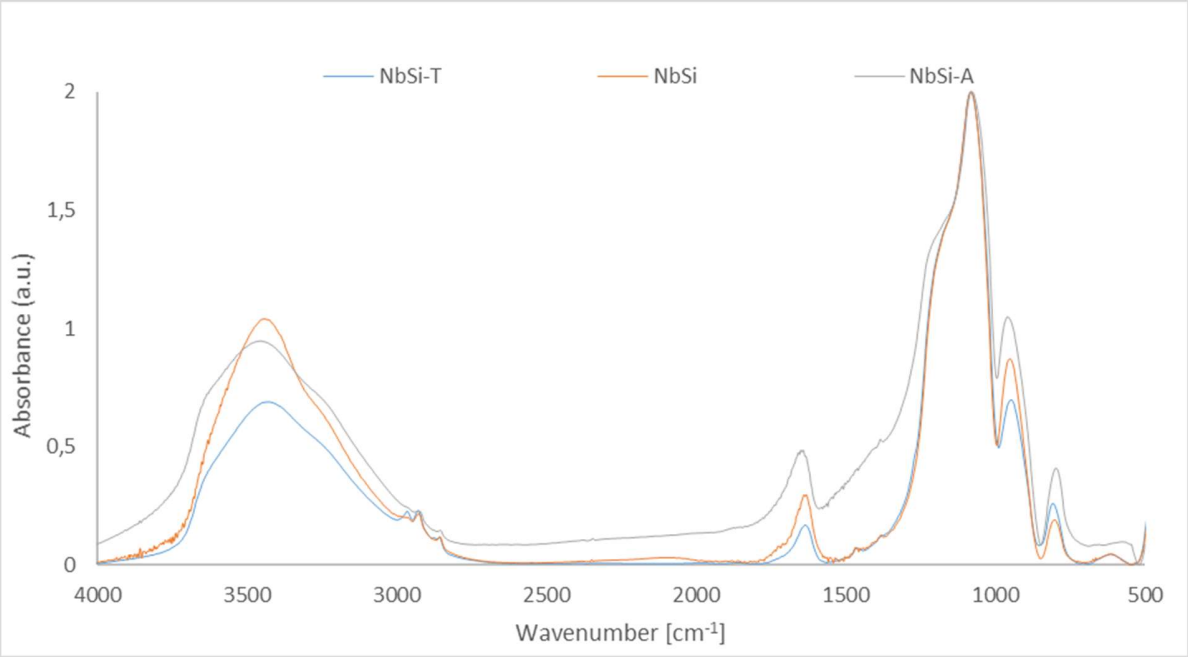

Figure 16 Absorbance of pristine samples measured by IR

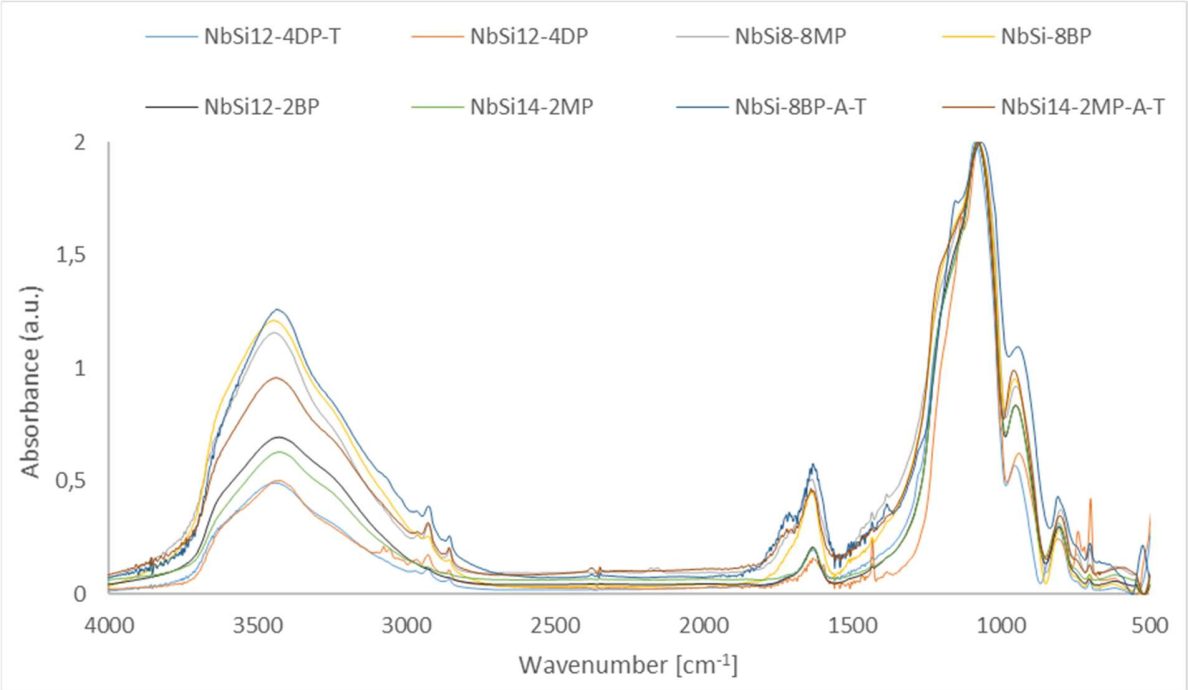

Figure 17 Absorbance of phenylated samples measured by IR

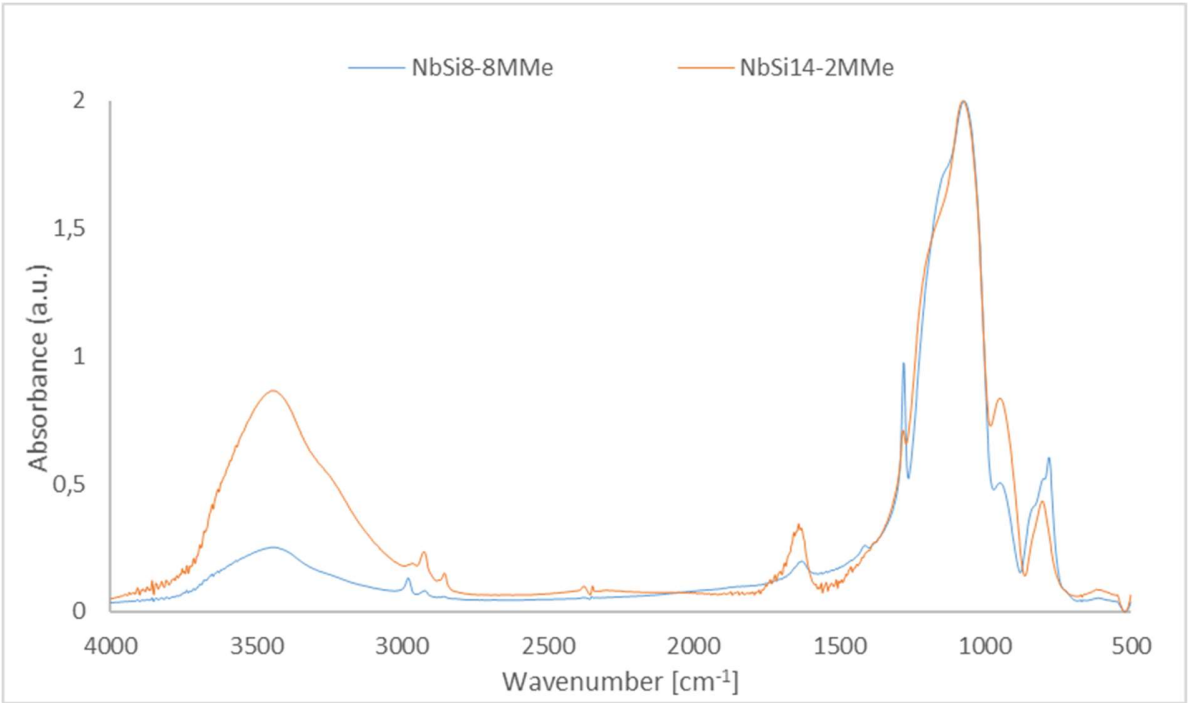

Figure 18 Absorbance of methylated samples measured by IR

Some general statement can be made for all samples. First of all, the C−H stretching band is visible in all spectra, even for the samples without any organic groups. Moreover, for almost all the phenylated samples, the C−H stretching band is below 3000 cm^{-1}, corresponding H atoms bound to aliphatic chains and not aromatic rings. This could either mean that it is an artefact from the instrument, there could also be some kind of oil residues in the analysis chamber. Besides, the spectra of phenylated samples exhibit some peaks characteristic for aromatic groups around 700 cm^{-1} (C−H bending band) and 1450 cm^{-1} (C−C stretching band).

KBr was used to make pellets because it has a transmittance of 100 % in the range of wavenumber 4000 to 400 cm^{-1}. Therefore, it should not show any absorption in this range. However, the KBr is a very hygroscopic salt, therefore all spectra have two characteristic bands corresponding to water. Indeed, the broad band above 3000 cm^{-1} corresponds to the O−H stretching band, whereas the 1630 cm^{-1} peak corresponds to the O−H bending band. These O−H bands are mostly those from the water caught by the KBr, but a small amount could also come from the silanols, adsorbed water and Nb−OH species that could be present at the surface of the sample.

The phenylated samples synthesized through the acetate route and calcined at 350 °C in order to protect the aromatic groups within the matrices show some particular peaks around 1700 cm^{-1} (*Figure 17*, samples **NbSi-8BPh-A-T** and **NbSi14-2MPh-A-T**) [50]. The literature has established that this double peak at 1630-1720 cm^{-1} corresponds to the stretching of C=O bonds. These C=O bonds should not be present in the samples, and may be caused by some residues of acetate groups from the synthesis. Therefore, the calcination temperature of 350 °C of the acetate samples does not seem to be high enough to burn all the organic residues from the synthesis. Going to higher temperature is nonetheless difficult as it would mean that more phenyl groups are lost during the calcination, which is why a compromise has to be found in further research (see results of TGA analysis below). Furthermore, since the acetate residues are resilient even after calcination at 350 °C, the measurement of incorporated organic species inside the hybrid could be altered by the presence of these residues.

Finally, samples with methyl moieties show an expected behavior. The particular Si–CH_3 peak is present in both samples at 1270 cm^{-1}, and the more methyl incorporated, the higher is the intensity of this peak (*Figure 18*).

3.4.2 TPD-MS

Beside its capacity to quantify the strength and the number of acid sites in a sample, the thermal desorption spectroscopy linked to a mass spectrometer can be a very interesting tool to characterize thermal stability of organic-inorganic hybrid materials. This technique is complementary to the thermogravimetric analysis. Whereas TGA gives a quantification of the organic moieties inside the hybrid, the nature of the incorporated organic species can be identified in TPD-MS.

A hypothesis that phenyl groups are leaving the sample in the form of benzene was suggested. The fragment ion of highest intensity to be formed from benzene (base peak) is at m/z= 78 and therefore this fragment was followed by TPD-MS. The temperature program used is the same as for the NH_3 desorption measurement. TPD-MS of all analyzed hybrid samples with phenyl groups are shown in Figure 19 and all of them display releases of ions with m/z = 78.

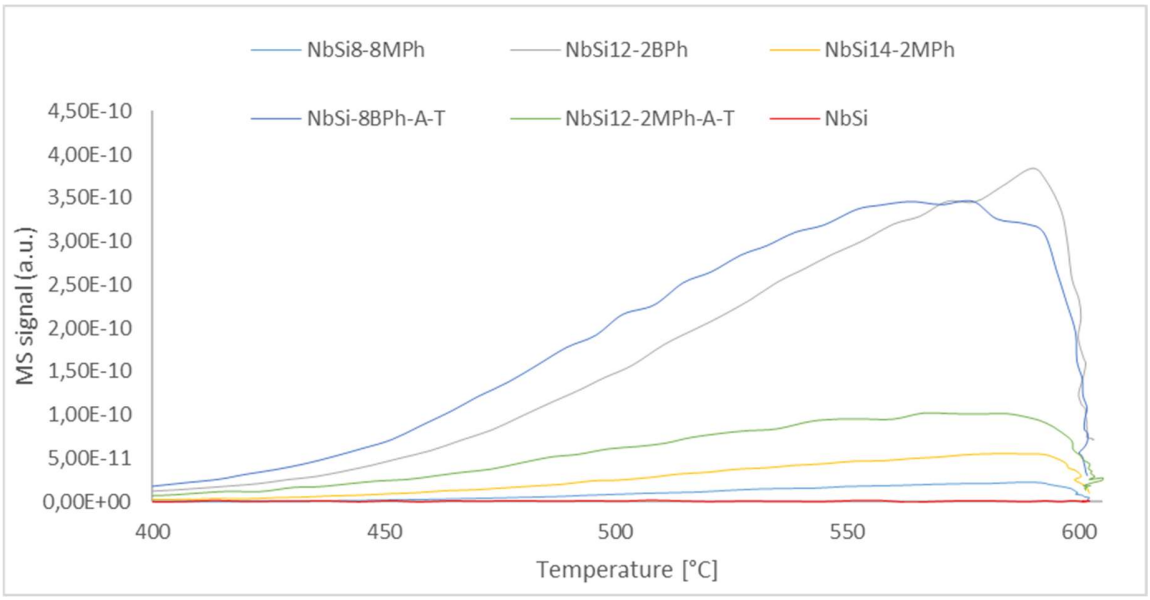

Figure 19 Intensity of m/z=78 as a function of the temperature, measured by TPD-MS

Figure 19 is useful to understand the actual stability of the incorporated phenyl groups. As expected, no signal for m/z=78 was observed in the sample without phenyl groups. It proves that phenyls are released from the samples from 400 °C to 600 °C. However, it is important to remember that analyzed samples are already calcined at 400 °C (350 °C for **NbSi-8BPh-A-T** and **NbSi12-2MPh-A-T**), and before the actual measurement, the samples are kept at 400 °C for an hour *(Figure 8*), thus most of the unstable groups is supposed to be gone. Moreover, the conditions of the analysis are different in NH_3-TPD (20 ml min^{-1} Ar + 20 ml min^{-1} He + 5% vol. ammonia) and in TGA (in air). Thus, the use of a TGA-MS should be considered for further research on the characterization of hybrid materials.

3.4.3 TGA

Hybridization was performed using organosilanes as silicon precursors, but quantification of the hydrophobic species in the framework is still required. Therefore, thermogravimetric analyses were performed with 3 objectives: (i) Verify the hydrophobicity of the samples, (ii) Quantify the organic content and (iii) Verify the thermal stability of the organic groups. The mass loss as a function of the temperature can be found in *Figure 20* (non-hybridized samples), *Figure 21* (phenylated samples) and *Figure 22* (methylated samples).

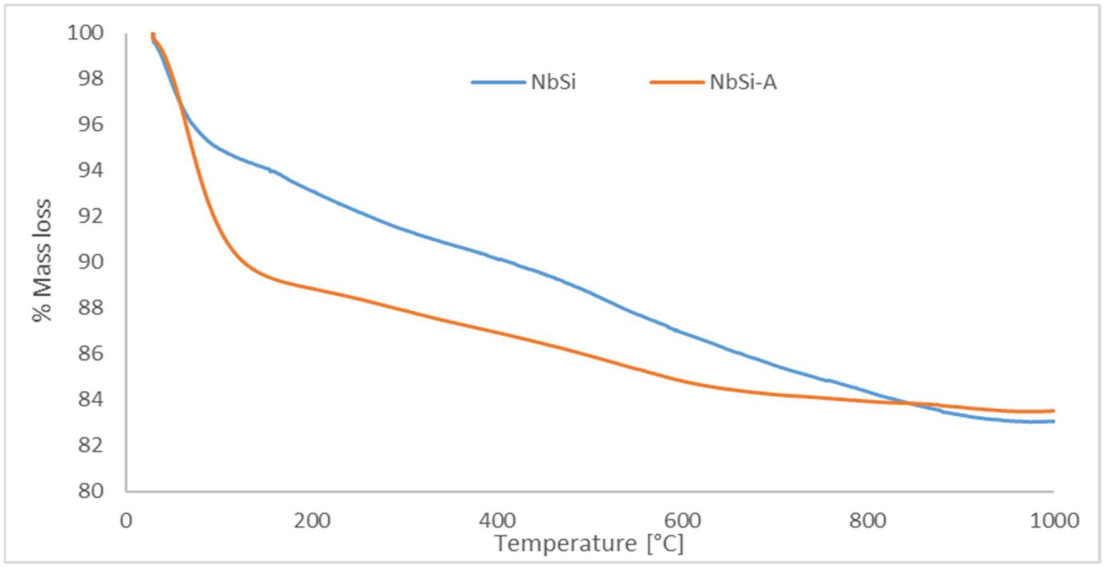

Figure 20 thermogravimetric analysis of pristine samples

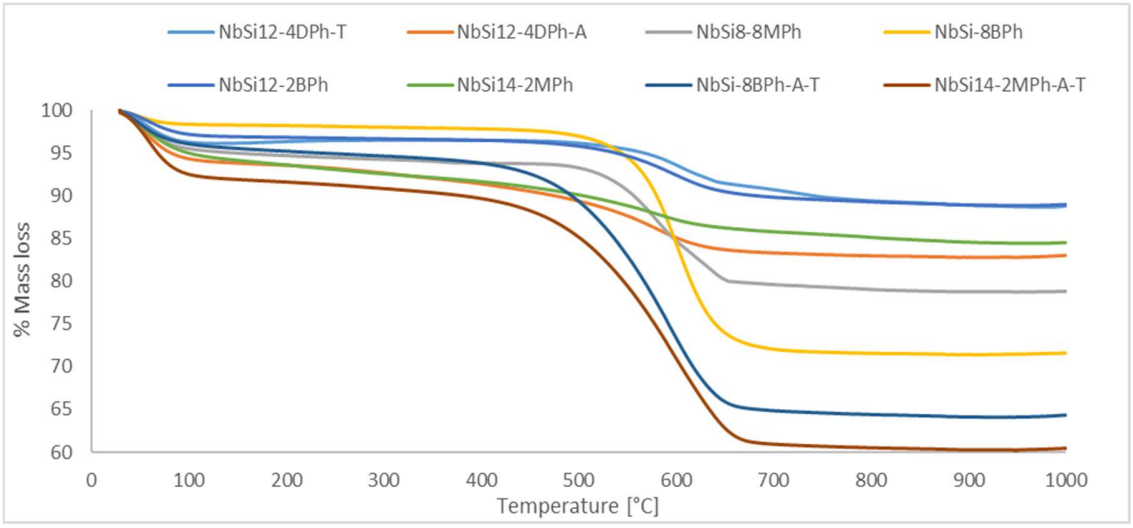

Figure 21 thermogravimetric analysis of phenyl samples

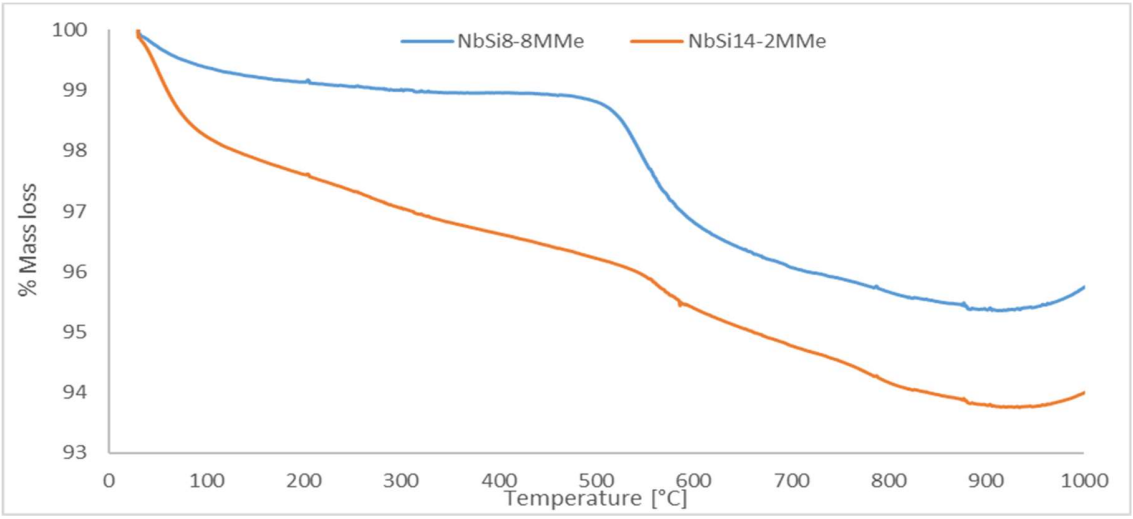

Figure 22 thermogravimetric analysis of methyl samples

All three figures have generally three distinct mass losses that could be associated with the loss of specific compounds. The first mass loss, in the temperature range from 0 to 100 °C, can be attributed the release of adsorbed water. It is interesting to note that usually, the higher the organic content, the lower the mass loss attributed to water. This perfectly makes sense as more organic groups means higher hydrophobicity of the sample. Based on the TPD-MS results, it is assumed that for phenylated samples, the second mass loss between 400 and 700 °C is

attributed to the phenyl groups oxidation. The similar hypothesis can be made for the methyl moieties, even though the verification should have been done with a mass spectrometer. Therefore, when comparison of experimental and theoretical mass loss will be presented, the experimental mass loss will refer to temperature range from 400 to 700 °C. The final mass loss related to temperatures higher than 700 °C can be attributed to the mass of unburned residues. The calculation of the expected mass loss related to the introduced organic moieties versus the actual experimental loss is displayed in *Table 6*.

Table 6 Theoretical versus experimental mass loss measured by TGA

	Experimental mass loss between 400 and 700 °C [%]	**Theoretical mass loss [%]**
NbSi-T	0	0
NbSi	1.1	0
NbSi-A	1.2	0
NbSi12-4DPh-T	5.3	34
NbSi12-4DPh	/	33
NbSi12-4DPh-A	7.6	35
NbSi8-8MPh	13	33
NbSi14-2MPh	5.6	12
NbSi14-2MPh-A-T	27	11
NbSi-8BPh	24	27
NbSi12-2BPh	6.3	9.7
NbSi-8BPh-A-T	28	31
NbSi8-8MMe	3.5	4.8
NbSi14-2MMe	0.85	0.67

In each hybrid sample, we actually observe a mass loss related to organic groups, which confirms that organic groups are indeed incorporated in the inorganic matrix. However, mass losses related to organic groups are systematically lower than the expected mass of organic moieties incorporated. This is due to the release of the organic groups during the calcination.

Samples without organic groups (**NbSi**, **NbSi-A**) feature a very small mass loss in the temperature range from 400 to 700 °C, probably coming from unburned impurities. Another information which emerges from the table is the low experimental mass loss of the diphenyl samples. This is again a clue which verifies the hypothesis in which the diphenylsilanes are less reactive organosilane precursors, thus decreasing the amount of incorporated organic charge.

Based on the analysis of the infrared spectra of the acetate samples, some acetate residues can still be found even after the calcination at 350 °C. The fact that sample **NbSi14-2MPh-A-T** has a mass loss three times higher than expected could be related to this issue. The residual acetate groups might even match the thermal stability of the phenyl moieties, thus being oxidized in the same temperature window. The mass loss attributed to the phenyl groups is therefore wrong in this scenario, as the impurities are also burned, which is why the experimental mass loss is higher than the expected value. Nonetheless, this explanation would also mean that the same issue would be reported to sample **NbSi-8BPh-A-T**. Following the hypothesis, the actual amount of phenyl incorporated would be significantly lower, as the mass loss in the range of 400 to 700 °C would also correspond to the oxidation of acetate residues. The fact the experimental value is close to the expected one is, therefore, a coincidence.

Methylated samples show a similar thermal resistance as samples containing phenyl groups, being oxidized in the same temperature range. It is interesting to note that the main mass loss takes place around 530 °C for sample **NbSi8-8MMe** which is the decomposition temperature of methylated silica reported in the literature [51].

3.4.4 Solid-state NMR

Additional evidence of the incorporation of the methyl groups deduced from TGA data and IR spectra was found in the solid-state NMR spectra of these hybrids. Different nuclei have been investigated during the measurement, as they bring different useful information. First, the ^{13}C CP MAS analysis exhibited one particular peak for both samples at 0 ppm, corresponding to methyl bound to silicon. The ^{29}Si MAS analysis has the purpose to compare signals of $MeSi(OSi)_3$

and $Si(OSi)_4$, and by integrating the data, the relative quantity of methyl groups can be found. The signal of $MeSi(OSi)_3$ is usually located at -60 ppm whereas the peak of $Si(OSi)_4$ is at -110 ppm [52]. The relative peak intensities can be found in *Table 7*.

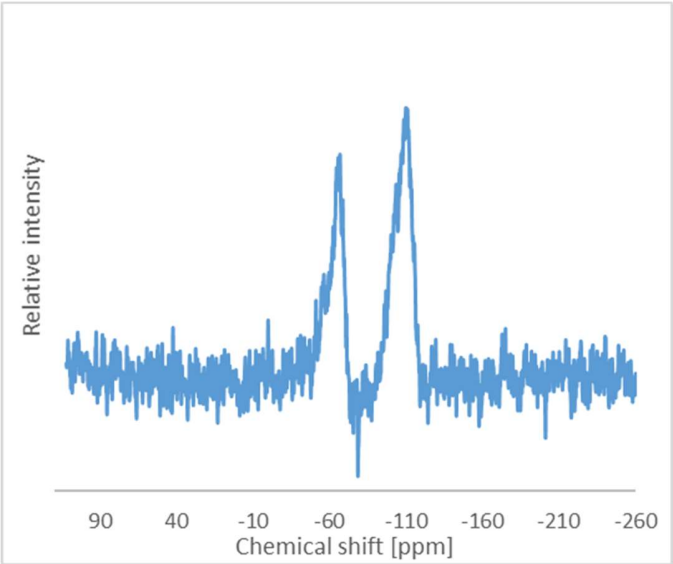

Figure 23 ^{29}Si MAS NMR of NbSi8-8MMe

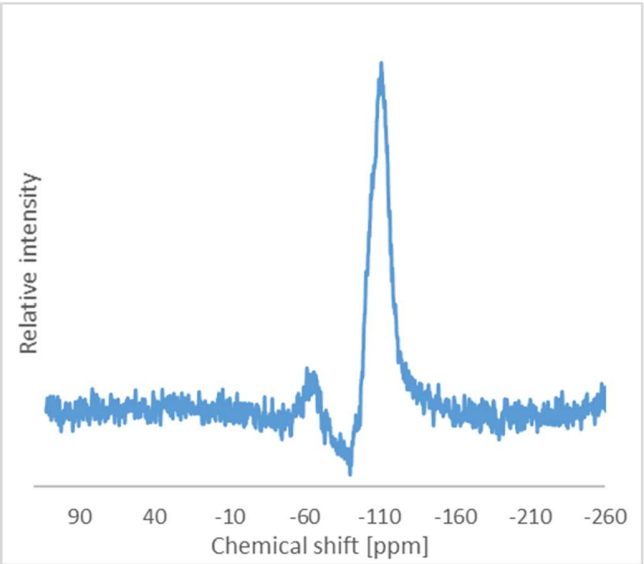

Figure 24 ^{29}Si MAS NMR of NbSi14-2MMe

Table 7 Integrated data of ^{29}Si MAS NMR of methyl samples

Sample	$MeSi(OSi)_3$ [%]	$Si(OSi)_4$ [%]	Expected percentage [%]
NbSi8-8MMe	38.2	61.8	50-50
NbSi14-2MMe	9.19	90.8	12.5-87.5

For both samples, the actual amount of methyl groups is lower than the expected one, meaning that as for the phenyls moieties, some methyls groups are lost during the calcination at 400 °C. A hypothesis on why the methyls are getting out before 400 °C is that the environnment during the calcination contains water that will hydrolyse the Si−C bond [53,54]. An improvement of the calcination method would be to pass the air flow during the calcination through water

catching agents to avoid sample hydrolysis. Another hypothesis would be simply that the reaction of $MeSiCl_3$ with the niobium intermediate has a low rate, yielding a less hybridized sample, as the remaining unreacted methyl moieties are leaving during the drying of the sample. This hypothesis can be verified by further measurements on uncalcined samples. If there are no difference between calcined and uncalcined samples, this hypothesis should also be taken into account.

3.5 Catalytic tests

The catalytic performances have been investigated in order to identify the consequences of the hybridization on the catalytic properties. Moreover, differences in the synthetic pathway could also lead to some changes in the activity. In order to quantify the activity of the catalysts, two main indicators will be considered: the ethanol conversion and the selectivity towards ethylene (*i.e.: targeted product*). Catalytic conversions of all measured samples are established in *Figure 25, Figure 26* and *Figure 27*.

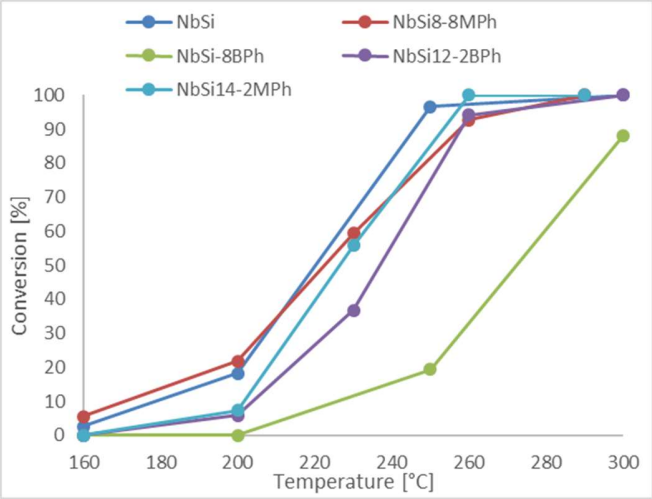

Figure 25 Catalytic conversions of alkyl halide samples (phenyls + reference)

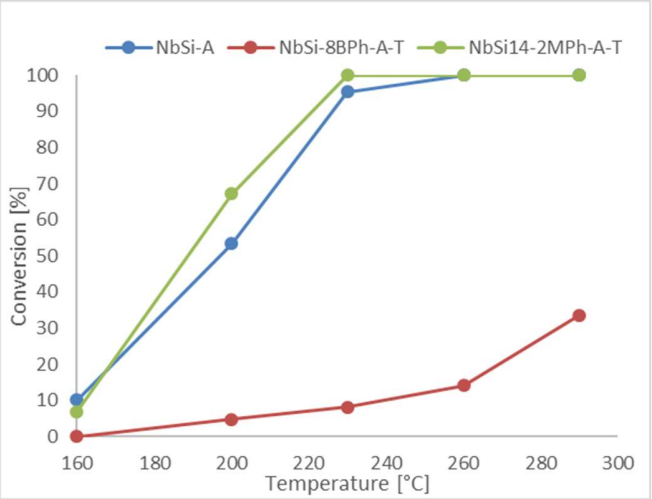

Figure 26 Catalytic conversions of acetate samples (phenyls + reference)

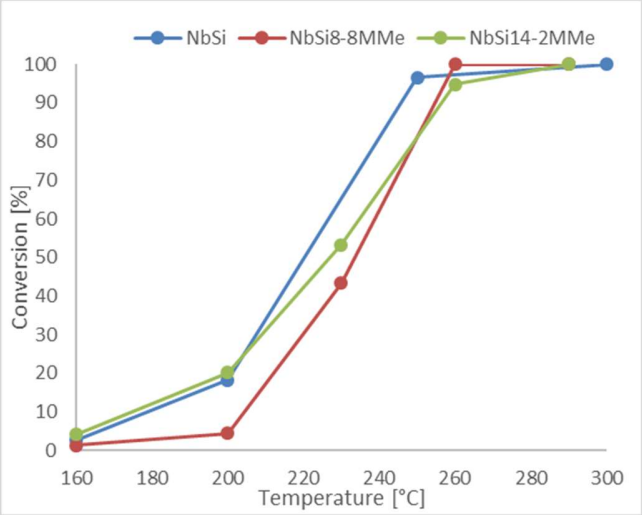

Figure 27 Catalytic conversions of alkyl halide samples (methyls + reference)

Considering all the light off curves, there is an overall trend towards the fact that the higher the content of organic groups, the less active the catalyst. This statement can apply to all the samples from both synthetic routes. Hybrid samples synthesized through the alkyl halide elimination route are usually less active than the pristine sample (**NbSi**). This result is supported by worse niobium incorporation of these samples that was deduced by IR and XPS analysis.

Phenylene-bridged hybrid samples synthesized by both routes (**NbSi-8BPh** and **NbSi-8BPh-A-T**) have the worst activity among all tested catalysts. High content of phenylene-bridging

moieties decrease strongly the overall performance of the catalysts. Nonetheless, TGA of these samples indicated that phenylene-bridged-silanes bring a large amount of incorporated organic mass and show TGA mass losses closest to the expected values. This is again an evidence of the fact that higher organic contents in the hybrid samples decrease their activity in ethanol dehydration.

Comparing both pristine and phenylated samples synthesized through the different routes can be also interesting, as there is clear difference of conversion over the temperature. As a matter of fact, beside **NbSi-8BPh-A-T**, samples from the acetate route exhibit a higher activity than their corresponding samples from the alkyl halide e. route. This comment is also approved by the analysis of both IR and XPS, as niobium in acetate samples is generally more homogeneously dispersed.

NbSi14-2MPh-A-T has the highest conversion, event better than its corresponding pristine catalyst. This supports the hypothesis in which acetate samples are more homogeneous thus more active. On the majority of the samples, adding organic moieties has a negative influence on their catalytic performances. However, this rule does not apply to this sample. This would suggest that there is an optimum to find in terms of nature and proportion of organic groups. In that case, low amount of pending-phenyl groups improves the ethanol conversion of the catalyst.

Performance measurements are not restricted to the analysis of the different catalyst conversions, as the focus of this study also covers the production of ethylene. To quantify this production, we will define the ethylene relative concentration (*Eq.22*)

$$\text{Ethylene relative concentration } [\%] = \frac{n_{ethylene}}{n_{ethylene}+n_{ethanol}+n_{diethylether}} 100 \quad (Eq.22)$$

Where:

- $n_{ethylene}$ is the number of moles of ethylene produced
- $n_{ethanol}$ is the number of moles of ethanol produced
- $n_{diethylether}$ is the number of moles of diethylether produced

The ethylene relative concentration will give an insight of the ethylene production with respect to the total production. The ethylene relative concentration as a function of the temperature in *Figure 28, Figure 29* and *Figure 30*.

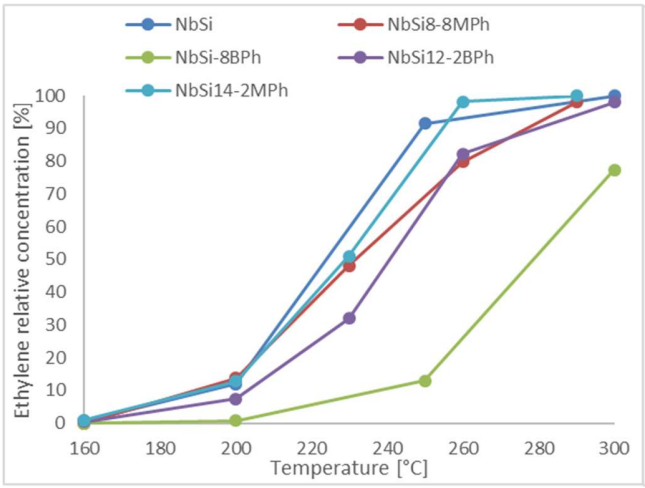

Figure 28 Relative percentage of ethylene production of alkyl halide e. samples (phenyls+ ref)

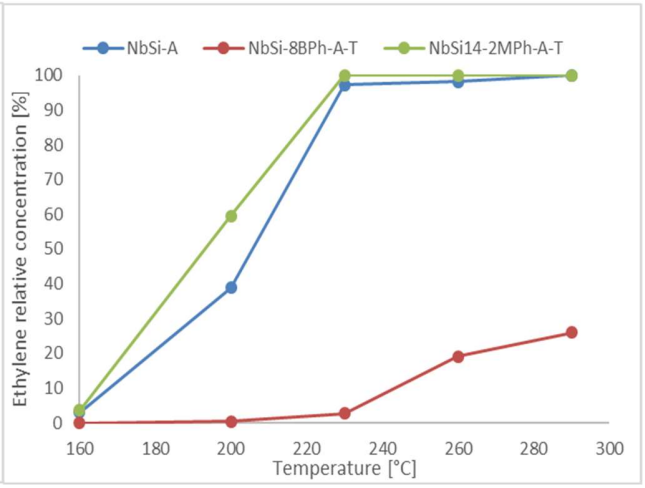

Figure 29 Relative percentage of ethylene production of acetate samples (phenyls+ ref)

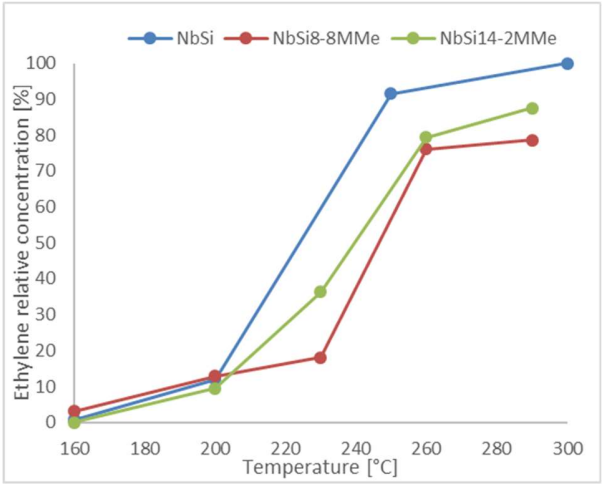

Figure 30 Relative percentage of ethylene production of alkyl halide e. samples (methyls + ref)

The ethylene relative concentration of each sample is globally similar to their conversion, except for methylated samples. Indeed, methyl groups seem to have a negative influence on the production of ethylene. In addition to that, the more methyl content, the less ethylene is produced.

3.6 Hydrothermal stability test

During the catalysis of some high phenyl content samples, an extra peak that has the same retention time as benzene has been discovered in the gas chromatogram. As phenyl instability was discovered by exposing the samples to a high water-content environment, a test has been proposed to identify the origin of this problem. Before the usual hydrothermal test, **NbSi-8BPh** (27 % in mass of phenyl content) sample has been set inside the reactor at 350 °C because this sample showed particular high benzene peaks (at 290 °C) during the catalysis. The same amount of catalyst as during catalysis and hydrothermal treatment was weighted and placed inside the reactor. Then, the sample has been subjected to a flow of the different components separately, and the stream was analyzed by GC to identify what was causing the apparition of the benzene peak. First, nitrogen was tested (40 ml min^{-1}) then ethylene diluted in nitrogen (0.93 ml min^{-1}, molar ratio: 0.0233) and finally water in nitrogen (0.216 g h^{-1}, molar ratio: 0.177). The results of this experiment can be found in *Figure 31*.

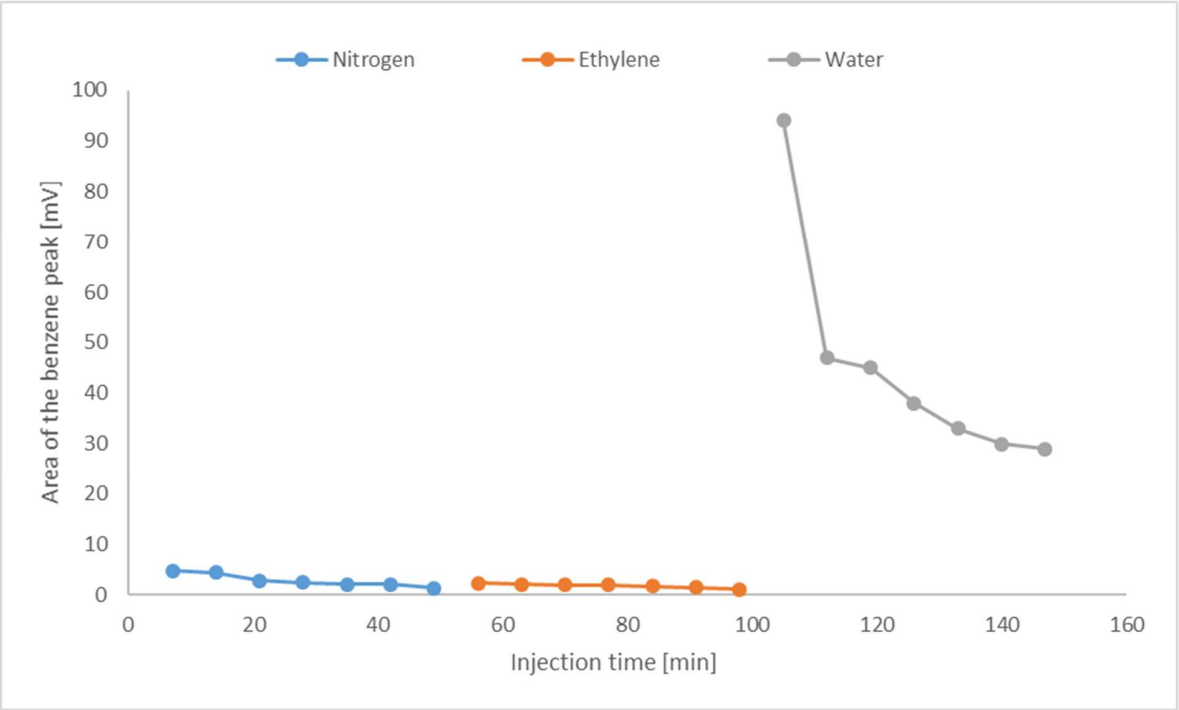

Figure 31 Measure of the area of the benzene peak in GC with NbSi-8BPh at 350 °C.

Overall, the benzene peak is detectable for all components, but what really stands out of this test is that water seems to be the one component that has the most harmful effect on the bridging-phenylene sample. In fact, phenylene-bridged organosilicas cleavage by water was already reported in literature [54].

The Si–C bond is moderately polar (Pauling electronegativities indicate that there is 12 % ionic character in the direction of C–Si^+), thus is relatively easily attacked by ionic reagent. Literature has already studied the case of the nucleophilic cleavage of carbon-silicon bonds with water as the nucleophilic reagent [53-55]. Inspired by the similar cleavage mechanism proposed in the literature, a mechanism of pending phenyl-silicon bond cleavage by water is suggested here. The mechanism involves a rate-determining synchronous attack of the nucleophile and a separation of the carbanion (*Eq.23*), which then quickly subtracts a proton from water (*Eq.24)*.

$$HO^- + (OSi)_3SiC_6H_5 \rightarrow [HO \dots Si(OSi)_3 \dots C_6H_5]^- \rightarrow HOSi(OSi)_3 + {C_6H_5}^- \quad (Eq.23)$$

$$H_2O + {C_6H_5}^- \rightarrow HO^- + C_6H_6 \quad (Eq.24)$$

The proposed mechanism involves the formation of the $C_6H_5^-$ carbanion (*Eq.23)*. As this specie is highly unstable because of the lack of substitution groups, the first reaction will be less likely to happen. That is why it is reported that phenyl groups are usually cleaved from silicon with difficulty by common nucleophilic agents [56]. This might explain why phenyls well incorporated are unstable only in conditions with very high water content and temperature of at least 290 °C.

3.7 Stability of the organic moieties

Now that the instability of the hybrids in high water content atmosphere has been highlighted, extensive studies on the stability in hydrothermal conditions of the sample could indicate which organic moieties are the most resilient. Stabilities of different organic loadings will be discussed through (i) BET, (ii) IR, (iii) solid-state NMR and (iv) TGA.

3.7.1 Textural properties alteration

An insight on the consequence of the exposition of the catalyst to high water concentration is reported in *Table 8* (specific surface area) and in *Table 9* (pore volume).

Table 8 BET measurements of post-test samples specific surface area

Sample	SSA after calcination [$m^2\ g^{-1}$]	SSA after catalysis [$m^2\ g^{-1}$]	Loss [%]	SSA after HT [$m^2\ g^{-1}$]	Loss [%]
NbSi-T	830	/	/	/	/
NbSi	690	560	18.8	700	-1.5
NbSi-A	700	620	11.4	390	44.3
NbSi12-4DPh	600	/	/	/	/
NbSi12-4DPh-A	910	/	/	/	/
NbSi8-8MPh	610	570	6.5	510	16.4
NbSi14-2MPh	630	340	46	610	3.2
NbSi14-2MPh-A-T	720	550	23.6	630	12.5
NbSi-8BPh	1030	570	44.7	690	33
NbSi12-2BPh	660	690	-4.5	710	-7.6
NbSi-8BPh-A-T	670	550	17.9	310	53.7
NbSi8-8MMe	690	600	13	250	63.8
NbSi14-2MMe	770	670	13	690	10.4

Table 9 measurements of post-test samples pore volume

Sample	PV after calcination [$cm^3\ g^{-1}$]	PV after catalysis [$cm^3\ g^{-1}$]	Loss [%]	PV after HT [$cm^3\ g^{-1}$]	Loss [%]
NbSi-T	2.59	/	/	/	/
NbSi	1.29	0.634	50.9	1.28	0.775
NbSi-A	0.266	0.624	-134	0.184	30.8
NbSi12-4DPh-T	/	/	/	/	/
NbSi12-4DPh	1.24	/	/	/	/
NbSi12-4DPh-A	0.614	/	/	/	/
NbSi8-8MPh	0.396	0.473	-19.4	0.410	-3.54
NbSi14-2MPh	0.587	0.274	53.3	0.646	-10.1
NbSi14-2MPh-A-T	1.12	0.628	43.9	0.868	22.5
NbSi-8BPh	1.62	0.683	57.8	0.903	44.3
NbSi12-2BPh	0.604	0.732	21.2	0.550	8.94
NbSi-8BPh-A-T	0.875	0.274	68.7	0.194	77.8
NbSi8-8MMe	2.27	1.66	26.9	0.957	57.8
NbSi14-2MMe	1.27	1.10	13.4	1.16	8.66

Textural properties of samples after hydrothermal treatment will be preferably discussed over data after catalysis because the HT conditions remained exactly the same for all samples (*c.f.:2.2.6.2*).

Previous studies have already reported hydrothermal stability tests on niobium doped silica SBA-15 (non-hybridized). This test compares the textural evolution between two different niobium doped SBA-15 exposed to a steam flow at 600 °C. The textural properties of the doped solid with a molar ratio Si/Nb of 10 was affected, while the texture of the other doped solid with a molar ratio Si/Nb of 5 did not change [57]. This suggests that the addition of heteroatoms with a sufficient content makes it possible to improve the hydrothermal stability of the silica. However, a compromise has to be found, as higher loading of niobium would influence the dispersion and the nature of the acid sites.

Beside **NbSi-A**, samples with larger amount of organic species incorporated (calculated by TGA) loose eventually more specific surface area and pore volume than the other samples. Since the cleavage of the Si−C has been evoked, the cause of the loss of textural properties is identified. The more organic content, the more organic moieties are cleaved and the higher the impact on the textural properties. This trend is similar after catalysis, suggesting again that the water produced by the reaction is sufficient for the hydrolysis of the silicon-carbon bond. Methylated samples show an overall higher resistance of textural properties against water.

In some cases the specific surface area (*i.e.:* **NbSi12-2BPh**) and the pore volume (*i.e.:* **NbSi8-8MPh**) increase after exposition to water. This suggests that the cleavage of Si−C bond is not the only phenomena that happens during the exposition to water. Hydrolysis of Si−O−Si and Si−O−Nb bridges can appear, thus implying the splitting of this bridge yielding two silanol sites [58]. Moreover, it can transform the Lewis acid sites NbO_4 into Brønsted sites, thus influence the activity of the catalysts. Nevertheless, the hydrolysis of oxo-bridges imply an increased surface area and pore volume, which could explain why some samples have improved textural properties after tests.

3.7.2 Infrared analysis of methylated samples after HT

The purpose of this analysis is to identify whether the methyl groups are cleaved in the same way as the phenyl moieties by analyzing peak intensity at 1270 cm^{-1}, which is related to deformation vibrations of $Si-CH_3$ groups. Spectra of both methylated samples before and after HT are shown in *Figure 32* (**NbSi8-8MMe**) and *Figure 33* (**NbSi14-2MMe**).

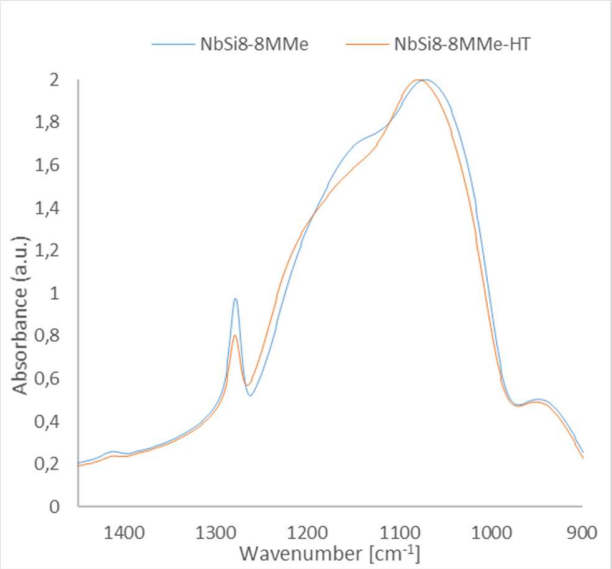

Figure 32 IR spectrum of sample NbSi8-8MMe before and after HT

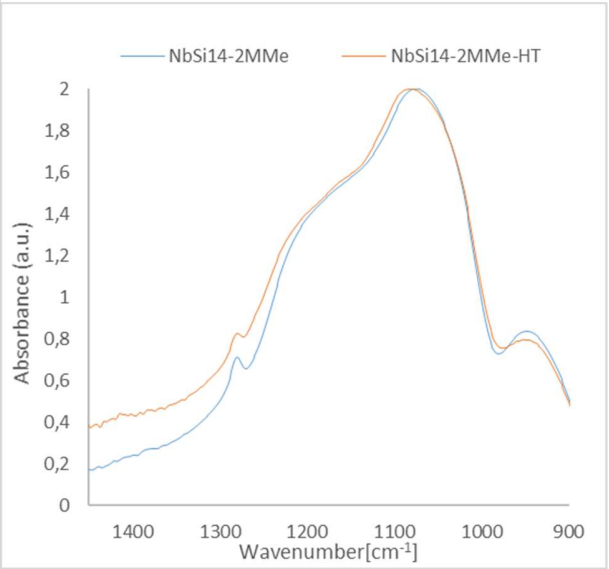

Figure 33 IR spectrum of sample NbSi14-2MMe before and after HT

Comparing the two spectra, the difference in intensity of the Si−CH_3 peak follows the predictions, as the sample with more methyl content (**NbSi8-8MMe**) has a higher peak intensity than the other. When it comes to the intensity before and after treatment, both spectra show that the samples after hydrothermal test have lost a significant amount of Si−CH_3 species. Now that the loss of Si−CH_3 has been established, the quantification can be made by solid-state NMR and thermogravimetric analysis.

3.7.3 ^{29}Si Solid-state NMR of NbSi14-MMe after HT

The methyl loss was investigated in sample **NbSi14-MMe** by ^{29}Si solid-state NMR. The point of this experiment was to highlight and quantify the loss of the methyl groups during the hydrothermal stability treatment. The ^{29}Si MAS NMR spectrum of this sample after HT is exhibited in *Figure 34*. Peaks were integrated and compared to the sample before the hydrothermal treatment in *Table 10*.

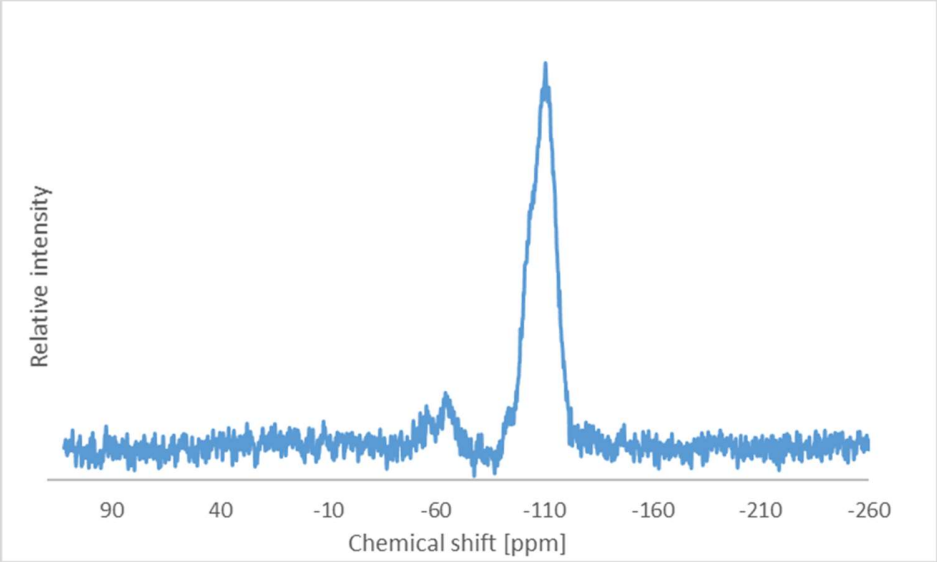

Figure 34 ^{29}Si SS NMR of NbSi14-2MMe after HT

Table 10 Methyl loss during HT of sample NbSi14-2MMe measure by ^{29}Si SS NMR

Sample	$MeSi(OSi)_3$ [%]	$Si(OSi)_4$ [%]
NbSi14-2MMe	9.19	90.8
NbSi14-2MMe-HT	7.26	92.7

From the integration we can observe a decrease in content of $MeSi(OSi)_3$ species from 9.19 to 7.26 % after the hydrothermal treatment. In other words, it means that 21 % of all methyl groups were lost during hydrothermal treatment. This result is supported by the infrared spectra of **NbSi14-2MMe**, where the scission of Si−C bond during the treatment is clearly visible. Thus, pending-methyl groups in sample **NbSi14-2MMe** seem to be unstable in high water concentration as well, where the cleavage of methyl-silicon is probably also related to the nucleophile attack of water as it is in the case of the phenyl-silicon bond [53].

3.7.4 TGA of samples after hydrothermal treatment

In order to quantify the loss associated with the cleavage of the Si−C bond, thermogravimetric analyses were performed after hydrothermal treatment. These results are presented in *Table 11* and should give a picture of the global hydrothermal resistance of the different organic moieties.

Table 11 Comparison of mass loss before and after hydrothermal treatment

Sample	Mass loss after calcination [%]	Mass loss after hydrothermal treatment [%]
NbSi8-8MPh	13	5.5
NbSi14-2MPh	5.6	2.3
NbSi14-2MPh-A-T	27	5.3
NbSi-8BPh	24	6.2
NbSi-8BPh-A-T	28	11
NbSi8-8MMe	3.5	1.9

Large differences between mass losses before and after hydrothermal treatment are recorded, thus confirming again the loss of organic groups and the instability of the hybrids in these conditions. Higher organic content also mean higher loss during the exposition to high water concentration, meaning that further research on these hybrids should be investigated with lower amount of organic species. Concerning the samples synthesized through the acetate method, acetate impurities can react with water yielding undesired products (e.g.: carbonates). These unwanted species could be trapped in the pores, thus needing harsher conditions to be oxidized. The remaining species that are oxidized between 400 and 700 °C are thus not only composed of phenyl moieties but also of impurities.

3.7.5 Comparison of phenyl and methyl groups stability

A clear comparison between the stability of methylated and phenylated sample is the first step toward the establishment of future perspectives. From all post-test characterization, it is known that both phenyl and methyl groups are unstable in high water concentration. Actually, the loss of organic groups is more related to the initial content more than on its nature. Nonetheless, in general the loss of phenyl groups during the hydrothermal treatment seem slightly higher than the loss of corresponding methylated sample.

To seek a higher stability, lower content of organic groups should be considered. Methyl groups should be prioritized over phenyl ones, but a tremendous amount of different organosilane precursors exists and should also be investigated in further research on hybrid stability under hydrothermal conditions.

4. Conclusions

This project aims to synthesize new solid organic-inorganic hybrid Nb_2O_5-SiO_2 mixed-oxide catalysts efficient in the dehydration of ethanol. The preparation of these materials was carried out by novel non-hydrolytic sol-gel process, which produces homogeneous and mesoporous solids with high specific surface areas. Polycondensation reactions were based on two different synthetic pathways: (i) the alkyl halide elimination route and (ii) the acetate route. The incorporation of niobium was successfully achieved by both synthetic routes, but the acetate pathway has shown a slightly better homogeneity of niobium dispersion in silica. Both routes yielded mesoporous high specific surface area materials with excellent textural properties.

The introduction of organic groups inside mixed-oxides was deeply studied. The hybridization of Nb_2O_5-SiO_2 mixed-oxide had two purposes. First, it would provide an improved stability of the framework in high water concentration environment because carbon-carbon bonds are more stable against hydrolysis reactions. Secondly, hydrophobic hybrids would enhance the desorption of water yielded by the dehydration, thus would influence the activity of the catalysts. Several types of organic compound such as phenyl, diphenyl, phenylene-bridging and methyl groups were tested during the preparation. In all cases, the incorporation of organic groups inside inorganic matrices was achieved. However, significant amounts of organic groups are lost during the calcination at 350 or 400 °C in all hybrid samples. Methylated samples after calcination showed an improved resistance against the temperature.

The ethylene production through dehydration process was a central part of this work, thus catalytic tests have been studied. Samples produced through the acetate pathway display higher conversions than samples from the alkyl halide elimination route. It was also found out that high organic content in hybridized samples decrease the conversion of ethanol. All types of organic compounds integrated in hybrids behave similarly, except for methyl moieties that have a relatively good conversion but show also lower ethylene production.

Finally, one of the objective was to enhance the hydrothermal stability of the samples. When the hybrid samples were exposed to the hydrothermal stability test, high losses of surface

area and pore volume were recorded. Further investigations proved the hydrolysis of the silicon-carbon bond. All types of organic compounds have been shown unstable against water, however methylated samples are slightly more resistant than the materials with incorporated phenyl groups. The results open the ways of future research concerning hybrid materials in presence of water.

5. Perspectives

Hereafter, some suggestions for improvement in future research on hybrids of Nb_2O_5-SiO_2 mixed-oxides will be presented. Then, further research will be proposed in a contextual perspective.

Non-hydrolytic sol-gel process is not limited to two synthetic routes, but is actually much wider than that. Other synthetic pathways should be explored such as the ester elimination for instance. The ester elimination has already been studied for the hybridization of silicon phosphates oxides [52]. On the other hand, acetamide route could also be considered and directly compared to its derivative, the acetate route [59].

More interest in the hybrids should be considered as well. Since high organic contents (>10 % in mass) lead to unstable materials in catalytic conditions, lower amount of organosilane precursors should be added during the preparation. Other type of organosilanes, especially bridging-units, should obviously be tested in the hybrids, as it could contribute also to improve the mastering of the pore size [60].

Regarding the stability of the hybrids towards high water concentration, synthesized materials should be exposed to more diverse hydrothermal conditions by changing the temperature and the composition in water of the inlet stream. Furthermore, in a more contextual perspective, conditions similar to those used in industry would give a better insight of the actual stability of these hybrids in industrial application. Along with this, mixtures of ethanol and water should be used during catalysis to get closer to the industrial conditions. Nonetheless, we are still far from the actual industrial applications as more research effort should be carried out towards reusability of the catalyst and the scaling-up of the process.

6. References

[1] Bender M. ,2000. Potential conservation of biomass in the production of synthetic organics. Resources conservation and recycling. Resources, Conservation and Recycling, 2000, Vol. 30, 49-58.

[2] Dias De Oliveira, M.E., Vaughan, B.E., Rykiel, E.J., 2005. Ethanol as Fuel: Energy, Carbon Dioxide Balances, and Ecological Footprint. BioScience 55, 593.

[3] Guo, M., Song, W., Buhain, J., 2015. Bioenergy and biofuels: History, status, and perspective. Renewable and Sustainable Energy Reviews 42, 712–725.

[4] Havlík, P., Schneider, U.A., Schmid, E., Böttcher, H., Fritz, S., Skalský, R., Aoki, K., Cara, S.D., Kindermann, G., Kraxner, F., Leduc, S., McCallum, I., Mosnier, A., Sauer, T., Obersteiner, M., 2011. Global land-use implications of first and second generation biofuel targets. Energy Policy 39, 5690–5702.

[5] Mohsenzadeh, A., Zamani, A., Taherzadeh, M.J., 2017. Bioethylene Production from Ethanol: A Review and Techno-economical Evaluation. ChemBioEng Reviews 4, 75–91.

[6] Naik, S.N., Goud, V.V., Rout, P.K., Dalai, A.K., 2010. Production of first and second generation biofuels: A comprehensive review. Renewable and Sustainable Energy Reviews 14, 578–597.

[7] Donald M., 2008. A Note on Rising Food Prices. World Bank Policy Research Working Paper Series, 4682.

[8] Rostek, E., 2016. BIOFUELS OF FIRST AND SECOND GENERATION. Journal of KONES. Powertrain and Transport 23, 413–420.

[9] Simpson-Holley, M., Higson, A., Evans, G., 2007. Renewables: Bring on the biorefinery.

[10] Mohsenzadeh, A., Zamani, A., Taherzadeh, M.J., 2017. Bioethylene Production from Ethanol: A Review and Techno-economical Evaluation. ChemBioEng Reviews 4, 75–91.

[11] Triantafyllidis, K.S., Lappas, A.A., Stöcker, M. (Eds.), 2013. The role of catalysis for the sustainable production of bio-fuels and bio-chemicals, 1st ed. ed. Elsevier, Amsterdam ; Boston, 557-576.

[12] Gaigneaux E., 2016. Principes de catalyse hétérogène - Bloc 6, Louvain-la-Neuve, 2-5.

[13] Rose, M., 2013. Catalysis for the Conversion of Biomass and its Derivatives. (Max Planck Research Library for the History and Development of Knowledge.) Edited by Malte Behrens and Abhaya K. Datye. Angewandte Chemie International Edition 52, 9613–9613.

[14] Zhang, M., Yu, Y., 2013. Dehydration of Ethanol to Ethylene. Industrial & Engineering Chemistry Research 52, 9505–9514.

[15] Huber, G.W., Iborra, S., Corma, A., 2006. Synthesis of Transportation Fuels from Biomass: Chemistry, Catalysts, and Engineering. Chemical Reviews 106, 4044–4098.

[16] Dömö ka, M.; Totha, M.; Raskó b, J.; Erdo˝helyi, A. Adsorption and reactions of ethanol and ethanol−water mixture on alumina-supported Pt catalysts. Appl. Catal., B 2007, 69 (3−4), 262−272.

[17] Rajakumar, B.; Reddy, K. P. J.; Arunan, E. Thermal decomposition of 2-fluoroethanol: single pulse tube and ab initio studies. J. Phys. Chem. A. 2003, 107 (46), 9782−9793.

[18] Galvita, V. V.; Semin, G. L.; Belyaev, V. D.; Semikolenova, V. A.; Tsiakarasb, P.; Sobyanin, V. A. Synthesis gas production by steam reforming of ethanol. Appl. Catal., A 2001, 220 (1−2), 123−127.

[19] Brandão, P., Philippou, A., Rocha, J. et al., 2002. Dehydration of Alcohols by Microporous Niobium Silicate AM-11. Catalysis Letters 80 , 80-99

[20] Tanabe, K., 2003. Catalytic application of niobium compounds. Catalysis Today 78, 65–77.

[21] Feliczak-Guzik, A., Nowak, I., 2009. Mesoporous niobosilicates serving as catalysts for synthesis of fragrances. Catalysis Today 142, 288–292.

[22] Qi, H., Chen, H., Li, L., Zhu, G., Xu, N., 2012. Effect of Nb content on hydrothermal stability of a novel ethylene-bridged silsesquioxane molecular sieving membrane for H2/CO2 separation. Journal of Membrane Science 421–422, 190–200.

[23] Gao, X., Wachs, I.E., Wong, M.S., Ying, J.Y., 2001. Structural and Reactivity Properties of Nb-MCM-41: Comparison with That of Highly Dispersed Nb2O5/SiO2 Catalysts. Journal of Catalysis 203, 18–24.

[24] J.C. Védrine, G. Coudurier, A. Ouqour, P.G. Pries de Oliveira, 1996. Niobium oxide based materials as catalysts for acidic and partial oxidation type reactions. Catalysis Today 28, 3-15.

[25] Tielens, F., Shishido, T., Dzwigaj, S., 2010. What Do the Niobium Framework Sites Look Like in Redox Zeolites? A Combined Theoretical and Experimental Investigation. The Journal of Physical Chemistry C 114, 3140–3147.

[26] Ushikubo, T., 2000. Recent topics of research and development of catalysis by niobium and tantalum oxides. Catalysis Today 57, 331–338.

[27] Styskalik, A., Skoda, D., Barnes, C., Pinkas, J., 2017. The Power of Non-Hydrolytic Sol-Gel Chemistry: A Review. Catalysts 7, 168.

[28] Debecker, D.P., 2017. Innovative Sol-Gel Routes for the Bottom-up Preparation of Heterogeneous Catalysts. The Chemical Record.

[29] Danks, A.E., Hall, S.R., Schnepp, Z., 2016. The evolution of 'sol–gel' chemistry as a technique for materials synthesis. Materials Horizons 3, 91–112.

[30] E. Gaigneaux, D.E. De Vos, P.A. Jacobs, J.A. Martens, P. Ruiz, G. Poncelet, P. Grange, 2002. Scientific bases for the preperation of heterogeneous catalysts. Studies in Surface Science and Catalysis 143, Elsevier, Amsterdam, 149-165.

[31] Debecker, D.P., Mutin, P.H., 2012. Non-hydrolytic sol–gel routes to heterogeneous catalysts. Chemical Society Reviews 41, 3624.

[32] Vioux, A., 1997. Nonhydrolytic Sol−Gel Routes to Oxides. Chemistry of Materials 9, 2292–2299.

[33] Andrianainarivelo, M., Corriu, R.J.P., Leclercq, D., Mutin, P.H., Vioux, A., 1997. Non-hydrolytic sol–gel process: zirconium titanate gels. Journal of Materials Chemistry 7, 279–284.

[34] Corriu, R., Leclercq, D., Lefevre, P., Mutin, P.H., Vioux, A., 1992. Preparation of monolithic binary oxide gels by a nonhydrolytic sol-gel process. Chemistry of Materials 4, 961–963.

[35] Styskalik, A., Skoda, D., Pinkas, J., Mathur, S., 2012. Non-hydrolytic synthesis of titanosilicate xerogels by acetamide elimination and their use as epoxidation catalysts. Journal of Sol-Gel Science and Technology 63, 463–472.

[36] Faustini, M., Nicole, L., Ruiz-Hitzky, E., Sanchez, C., 2018. History of Organic-Inorganic Hybrid Materials: Prehistory, Art, Science, and Advanced Applications. Advanced Functional Materials 1704158.

[37] Schwertfeger, F., Hüsing, N., Schubert, U., 1994. Influence of the nature of organic groups on the properties of organically modified silica aerogels: Code: B6. Journal of Sol-Gel Science and Technology 2, 103–108.

[38] J. H. Balthis, E. G. Rochow and D. G. White, in Inorganic Syntheses, ed. J. C. B. Jr, John Wiley & Sons, Inc., 2007, pp. 45–47.

[39] Pomalaza, G., Capron, M., Ordomsky, V., Dumeignil, F., 2016. Recent Breakthroughs in the Conversion of Ethanol to Butadiene. Catalysts 6, 203.

[40] Alothman, Z., 2012. A Review: Fundamental Aspects of Silicate Mesoporous Materials. Materials 5, 2874–2902.

[41] Broekhoff, J.C.P. Mesopore determination from nitrogen sorption isotherms: Fundamentals, scope, limitations. Stud. Surf. Sci. Catal. 1979, 3, 663–684.

[42] B.J. Clapsaddle, A.E. Gash, J.H. Satcher Jr, R.L. Simpson, Silicon oxide in an iron(III) oxide matrix: the sol–gel synthesis and characterization of Fe–Si mixed oxide nanocomposites that contain iron oxide as the major phase, Journal of Non-Crystalline Solids, 331 (2003) 190-201.

[43] C.M. Parler, J.A. Ritter, M.D. Amiridis, Infrared spectroscopic study of sol–gel derived mixed metal oxides, Journal of Non-Crystalline Solids, 279 (2001), 119-125.

[44] Schraml-Marth, M., Walther, K.L., Wokaun, A., Handy, B.E., Baiker, A., 1992. Porous silica gels and TiO2/SiO2 mixed oxides prepared via the sol-gel process: characterization by spectroscopic techniques. Journal of Non-Crystalline Solids 143, 93–111.

[45] Corma, A., Llabrés i Xamena, F.X., Prestipino, C., Renz, M., Valencia, S., 2009. Water Resistant, Catalytically Active Nb and Ta Isolated Lewis Acid Sites, Homogeneously Distributed by Direct Synthesis in a Beta Zeolite. The Journal of Physical Chemistry C 113, 11306–11315.

[46] Aronne, A., Marenna, E., Califano, V., Fanelli, E., Pernice, P., Trifuoggi, M., Vergara, A., 2007. Sol–gel synthesis and structural characterization of niobium-silicon mixed-oxide nanocomposites. Journal of Sol-Gel Science and Technology 43, 193–204.

[47] Zhang, L., Ying, J.Y., 1997. Synthesis and characterization of mesoporous niobium-doped silica molecular sieves. AIChE Journal 43, 2793–2801.

[48] Ziolek, M., Sobczak, I., 2017. The role of niobium component in heterogeneous catalysts. Catalysis Today 285, 211–225.

[49] Smith, A.L., 1960. Infrared spectra-structure correlations for organosilicon compounds. Spectrochimica Acta 16, 87–105.

[50] Moon, J.H., Seo, J.S., Xu, Y., Yang, S., 2009. Direct fabrication of 3D silica-like microstructures from epoxy-functionalized polyhedral oligomeric silsesquioxane (POSS). Journal of Materials Chemistry 19, 46-87.

[51] Bae, J.-Y., Jang, J., Bae, B.-S., 2017. Transparent, thermally stable methyl siloxane hybrid materials using sol-gel synthesized vinyl-methyl oligosiloxane resin. Journal of Sol-Gel Science and Technology 82, 253–260.

[52] Styskalik, A., Skoda, D., Moravec, Z., Babiak, M., Barnes, C.E., Pinkas, J., 2015. Control of micro/mesoporosity in non-hydrolytic hybrid silicophosphate xerogels. Journal of Materials Chemistry A 3, 7477–7487.

[53] Seddon, A.B., Hunt, S., Rourke, J.P., Bruce, D.W., 1994. Cleavage of silicon-carbon bonds and relative rates of hydrolysis of ormosil precursors for optical materials. Advanced Materials for Optics and Electronics 4, 285–291.

[54] Eaborn, C., 1969. Some recent studies of the cleavage of carbon-silicon and related bonds. Pure and Applied Chemistry 19, 375–388.

[55] Asefa, T., MacLachlan, M.J., Grondey, H., Coombs, N., Ozin, G.A., 2000. Metamorphic Channels in Periodic Mesoporous Methylenesilica. Angewandte Chemie International Edition 39, 1808–1811.

[56] Price, C.C., Sowa, J.R., 1967. Reactions of silanes and sulfides with strong bases in dimethyl sulfoxide. The Journal of Organic Chemistry 32, 4126–4127.

[57] Xiong, H., Pham, H.N., Datye, A.K., 2014. Hydrothermally stable heterogeneous catalysts for conversion of biorenewables. Green Chem. 16, 4627–4643.

[58] Sahai, N., Rosso, K.M., 2006. Computational Molecular Basis for Improved Silica Surface Complexation Models, in: Interface Science and Technology. Elsevier, pp. 359–396.

[59] Skoda, D., Styskalik, A., Moravec, Z., Bezdicka, P., Barnes, C.E., Pinkas, J., 2015. Mesoporous titanosilicates by templated non-hydrolytic sol–gel reactions. Journal of Sol-Gel Science and Technology 74, 810–822.

[60] Park, S.S., Ha, C.-S., 2006. Organic–inorganic hybrid mesoporous silicas: functionalization, pore size, and morphology control. The Chemical Record 6, 32–42.

[61] Hay, J.N., Raval, H.M., 2001. Synthesis of Organic−Inorganic Hybrids via the Non-hydrolytic Sol−Gel Process. Chemistry of Materials 13, 3396–3403.

Dehydration of ethanol over hydrophobic hybrids of niobium-silica mixed-oxides prepared by non-hydrolytic sol-gel process

Présenté par Gautier Boogaerts

Résumé The production of bio-sourced compounds has been deeply investigated during the past few decades as an alternative to the petrochemical industry. Currently, the main pathway to produce ethylene, one of the most produced chemical compounds in the world, is through hydrocarbon cracking process. Because of the depletion of fossil fuel reserves and their harmful impact on the global warming, the use of biomass **ethanol catalytic dehydration** has been developed. Various heterogeneous catalysts for this dehydration reaction have been explored, but poor resistance in high water concentration was reported. However, new **niobium-silica mixed-oxides** (**Nb_2O_5-SiO_2**) materials in recent research have displayed high hydrothermal stability while showing good catalytic performance. In line with it, hybridization (*i.e.: incorporation of organic moieties*) of this promising catalyst has been investigated in this work to make it even more resistant against hydrolysis. Another suggested feature of **hydrophobic hybrids** is that water, created during dehydration reaction, would desorb easier from the surface of the solid and thus impact the catalytic activity.

In this study, novel preparation method, the **non-hydrolytic sol-gel** (**NHSG**) process has been applied as it largely improves the homogeneity of the synthesized solids, which is an important property of hybrid mixed-oxides. Furthermore, this particular technique usually produces mesoporous materials with high specific surface areas. Two synthetic NHSG pathways have been studied in this work: (i) the alkyl halide elimination and (ii) the acetate route. Hybridization was carried out during the NHSG process by adding different types of organosilane precursors directly into the reaction mixture. Tested organosilanes include aromatic and aliphatic moieties both terminal ($C_6H_5SiR_3$, $(C_6H_5)_2SiR_2$, CH_3SiR_3) and bridging ($R_3SiC_6H_4SiR_3$) (R=Cl (i),OAc (ii)). Different molar ratios of organic groups were used in order to see the influence of their amount on the properties of the material.

In order to understand the stability and the catalytic performances of the hybrids, their physico-chemical characterization has been performed. Surface analyses reported that all synthesized materials were mesoporous with high surface areas. Niobium was successfully incorporated in all cases, however samples from the acetate route have shown a slightly better homogeneity of niobium dispersion in silica. The overall homogeneity of Nb-Si mixing in hybrids samples decreased with higher loadings of organic groups.

A big part of this master's thesis has been devoted to the evaluation of the catalytic activities in the ethanol dehydration reaction. Samples produced through the acetate pathway display higher conversions than samples from the alkyl halide elimination route. It was found out that high organic content in hybrid catalysts decrease the conversion of ethanol. All types of organic compounds integrated in hybrids behave similarly, except for methylated samples which have a relatively good conversion but show lower ethylene production.

Another objective was to enhance the **hydrothermal stability** of the samples to make them more economically and ecologically interesting. Indeed, pure ethanol production implies several step of distillation to get rid of the water. If the catalyst stability was improved in presence of water, then these expensive unit operations would be avoided. Unfortunately, when the hybrid samples were exposed to water at 250 °C for 24 hr, significant losses of surface area and pore volumes were observed. Further research proved that the hydrolysis of the silicon-carbon bond takes place under these conditions. All types of organic compounds have been shown unstable against water, however methylated samples seem to be slightly more stable than catalysts with incorporated aromatic groups.

Année académique 2017-2018